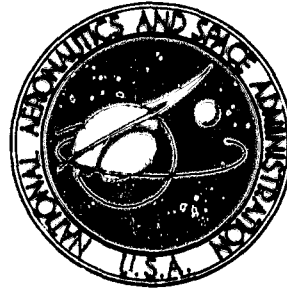


NASA TECHNICAL NOTE



NASA TN D-7855

NASA TN D-7855

(NASA-TN-D-7855) ANALYSIS OF BONDED JOINTS  
(NASA) 52 p HC \$4.25 CSSL 13E

N75-21673

H1/39 Unclass  
19048

# ANALYSIS OF BONDED JOINTS

*S. Srinivas*

*Langley Research Center*

*Hampton, Va. 23665*



1. Report No. NASA TN D-7855	2. Government Accession No.	3. Recipient's Catalog No.	
4. Title and Subtitle ANALYSIS OF BONDED JOINTS		5. Report Date April 1975	6. Performing Organization Code
		8. Performing Organization Report No. L-9563	10. Work Unit No. 501-22-02-01
7. Author(s) S. Srinivas	9. Performing Organization Name and Address NASA Langley Research Center Hampton, Va. 23665		11. Contract or Grant No.
12. Sponsoring Agency Name and Address National Aeronautics and Space Administration Washington, D.C. 20546			13. Type of Report and Period Covered Technical Note
		14. Sponsoring Agency Code	
15. Supplementary Notes Author was NRC-NASA Research Resident Associate, now at Argonne National Laboratory.			
16. Abstract A refined elastic analysis of bonded joints which accounts for transverse shear deformation and transverse normal stress was developed to obtain the stresses and displacements in the adherends and in the bond. The displacements were expanded in terms of polynomials in the thicknesswise coordinate; the coefficients of these polynomials were functions of the axial coordinate. The stress distribution was obtained in terms of these coefficients by using strain-displacement and stress-strain relations. The governing differential equations were obtained by integrating the equations of equilibrium. These differential equations were solved, and the boundary conditions (interface or support) were satisfied to complete the analysis.  Single-lap, flush, and double-lap joints were analyzed. The effects of adhesive properties, plate thicknesses, material properties, and plate taper on maximum peel and shear stresses in the bond were studied. Also, the results obtained by using the thin-beam analysis available in the literature were compared with the results obtained by using the refined analysis. In general, thin-beam analysis yielded reasonably accurate results, but in certain cases the errors were high. Numerical investigations showed that the maximum peel and shear stresses in the bond can be reduced by (1) using a combination of flexible and stiff bonds, (2) using stiffer lap plates, and (3) tapering the plates. Of the three joints considered, for a given total adhesive thickness and joint volume, the double-lap joint had the smallest maximum peel and shear stresses in the bond, whereas the flush joint had the highest.			
17. Key Words (Suggested by Author(s)) Joints Peel stress Adherends Bond		18. Distribution Statement Unclassified - Unlimited  New Subject Category 39	
19. Security Classif. (of this report) Unclassified	20. Security Classif. (of this page) Unclassified	21. No. of Pages 50	22. Price* \$3.75

## ANALYSIS OF BONDED JOINTS

S. Srinivas\*  
Langley Research Center

### SUMMARY

A refined elastic analysis of bonded joints which accounts for transverse shear deformation and transverse normal stress was developed to obtain the stresses and displacements in the adherends and in the bond. The displacements were expanded in terms of polynomials in the thicknesswise coordinate; the coefficients of these polynomials were functions of the axial coordinate. The stress distribution was obtained in terms of these coefficients by using strain-displacement and stress-strain relations. The governing differential equations were obtained by integrating the equations of equilibrium. These differential equations were solved, and the boundary conditions (interface or support) were satisfied to complete the analysis.

Single-lap, flush, and double-lap joints were analyzed. The effects of adhesive properties, plate thicknesses, material properties, and plate taper on maximum peel and shear stresses in the bond were studied. Also, the results obtained by using the thin-beam analysis available in the literature were compared with the results obtained by using the refined analysis. In general, thin-beam analysis yielded reasonably accurate results, but in certain cases the errors were high. Numerical investigations showed that the maximum peel and shear stresses in the bond can be reduced by (1) using a combination of flexible and stiff bonds, (2) using stiffer lap plates, and (3) tapering the plates. Of the three joints considered, for a given total adhesive thickness and joint volume, the double-lap joint had the smallest maximum peel and shear stresses in the bond, whereas the flush joint had the highest.

### INTRODUCTION

Bonded joints in primary structures are becoming increasingly common. In these joints, the adhesive which transfers the load from one member to another is subjected to a shear stress and a normal stress in the thickness direction (called peel stress). The joint, when subjected to static or fatigue loads, can fail from excessive shear or peel stresses in the bond. Thus, for a proper design of bonded joints, reasonably accurate estimates of the maximum peel and shear stresses in the bond are needed. Several papers

---

\*NRC-NASA Research Resident Associate, now at Argonne National Laboratory.

in the literature deal with the stress analysis of bonded joints. De Bruyne (ref. 1) analyzed single-lap joints but ignored the bending effects. Goland and Reissner (ref. 2) analyzed single-lap joints, taking into account large deflections. Erdogan and Ratwani (ref. 3) have analyzed the problem of a stepped joint but ignored the variation of stresses across the thickness (i.e., the bending effects). Wah (ref. 4) analyzed single-lap joints of anisotropic materials. Hart-Smith (ref. 5) has obtained the static failure loads for single-lap, double-lap, and scarf joints, taking into account plastic deformations in the adhesive. In all these references, the adherends were assumed to be thin beams; consequently, the transverse shear deformation and transverse normal stress were neglected. Neglecting these strains and stresses can cause errors in the stresses and displacements obtained by using thin-beam analysis.

In this paper a refined elastic analysis is developed in which the transverse shear deformation and the transverse normal stress are not neglected. The adhesive is assumed to be elastic. The accuracy of thin-beam analysis is assessed by comparing the bond stresses calculated from the thin-beam analysis with bond stresses calculated from the refined analysis. In addition, methods of reducing the maximum peel and shear stresses in the bond are studied. The configurations considered for analysis are double-lap, flush, and single-lap joints. The plates can be stepped or tapered and can be of composite material. Effects on maximum peel and shear stresses of thickness, modulus, and plate taper and of different adhesives along the length of the bond are studied.

#### SYMBOLS

$a^*(n)$  x-distance from origin to outer end of nth element (fig. 2)

$b^*(j)$  x-distance from origin to plate supports (fig. 2)

$\left. \begin{array}{l} C_{11}(j), C_{12}(j), \\ C_{22}(j), C_{33}(j) \end{array} \right\}$  elastic constants of jth plate

$c^*(n)$  thickness of nth element of plate 1 (fig. 2(a)) in single-lap joint

$\left. \begin{array}{l} D_{11}, D_{12}, \\ D_{22}, D_{33} \end{array} \right\}$  generalized rigidities (see eqs. (20))

$d^*(s)$  thickness of sth segment of plate 1 (see appendix A)

$e^*(s)$	distance from neutral axis of compound beam to top surface of sth segment of plate 1
$E_f^*(j)$	longitudinal Young's modulus of fiber in fiber-reinforced composite plates
$E_g^*$	adhesive Young's modulus in thickness direction
$F$	arbitrary constant
$f^*(s)$	thickness of sth segment of plate 2 (see appendix A)
$G_g^*$	adhesive shear modulus
$H_b^*$	thickness of plate 2 at inner end B in a double-lap joint (fig. 8(c))
$H_e^*$	thickness at ends A and B of plates 1 and 2 in single-lap joint (fig. 8(a)); thickness of plate 2 at A in double-lap joint (fig. 8(c))
$h^*(n)$	thickness of nth element of plate 2 (fig. 2)
$K^*(s)$	bending stiffness of sth segment (appendix A)
$k$	power of $Z$ in weighting function $Z^k$ (see eq. (15))
$k_x^*, k_z^*$	spring constants of bond in x- and z-direction, respectively
$k_x$	$= k_x^* t^*$
$k_z$	$= k_z^* t^*$
$L^*$	total length of joint, $b^*(1) + b^*(2)$ (fig. 2)
$l^*$	length of lap region (fig. 1)
$l_s^*$	length of stiff adhesive (fig. 7)
$M$	bending moment
$m$	number of steps

N	integral of direct stress $\sigma_x$
P	applied load on joint at end C per unit width (fig. 1)
p	applied stress at end C, $P/t^*$
Q	integral of shear stress $\sigma_{xz}$
R	vertical reaction at supports (fig. 9)
r	number of elements in lap region ( $r \geq 2$ )
S	shear force
$t^*$	thickness of overhang 1 in single-lap and double joints or half-thickness of overhang 1 in double-lap joints (fig. 1)
$u(j)$	displacement in x-direction of jth plate
V	integral of direct stress $\sigma_z$
$w(j)$	displacement in z-direction of jth plate
X	$= x/t^*$
x,z	coordinates
Z	$= z/t^*$
$\epsilon_x, \epsilon_z, \epsilon_{xz}$	strains in plates
$\zeta^*$	deflection, measured from neutral axis in large deflection analysis of single-lap joints (fig. 9)
$\eta^*$	adhesive thickness
$\mu^*(s)$	distance from neutral axis to reference axis in large deflection analysis of single-lap joints (fig. 9)

- $\xi^*$  axial coordinate used in large deflection analysis (fig. 9)
- $\sigma$  direct stress in thickness direction in bond; referred to as peel stress when it is tensile
- $\sigma_x, \sigma_z, \sigma_{xz}$  stresses in plates
- $\tau$  shear stress in bond
- $\phi$  functions of  $x$  occurring in expansion of  $u$ -displacement in  $z$ -coordinate
- $\psi$  functions of  $x$  occurring in expansion of  $w$ -displacement in  $z$ -coordinate

**Indices:**

- $i$  used in expansion of displacements in  $z$ -direction (see eqs. (1) and (2))
- $j$  plate, where  $j = 1, 2$
- $n$  element, where  $n = 1, 2, \dots, r$
- $s$  segment (see appendix A), where  $s = 1, 2, \dots, m + 2$

An asterisk denotes a dimensional quantity.

All linear dimensions are nondimensionalized by dividing by  $t^*$  and are then written without the asterisk; for example,  $a^*(n)/t^* = a(n)$ .

All elastic moduli are nondimensionalized by dividing by  $E_f^*(1)$ , the Young's modulus of the fiber in plate 1, and are then written without the asterisk; for example,  $E_f^*(2)/E_f^*(1) = E_f(2)$ .

A prime denotes differentiation with respect to  $X$ .

Numbers in parentheses are indices.

## ANALYSIS

The three types of joints considered are single lap, flush, and double lap. (See fig. 1.) In a single-lap joint, the two main plates, which are constant, tapered, or stepped in thickness, are joined by bonding them directly. In a flush joint, the two main plates are joined by bonding a lap plate on one side only. In a double-lap joint, the two main

plates are joined by bonding two plates – one on each side. In double-lap and flush joints the main plates are of constant thickness, whereas the lap plate or plates are constant, tapered, or stepped in thickness.

For the purpose of this analysis, tapered plates are idealized as stepped plates. The analysis is applicable for cases in which there are debonds. In the analysis, the joints are split into two regions, lap and overhang (see fig. 2). The lap region is further split into a number of smaller elements, depending on the number of steps and presence of debond. Plate thickness and material properties are assumed to be constant within each element. For example, in figure 2, where the joint has four steps, the lap region is treated as four bonded elements (1, 2, 5, and 6) and two unbonded elements (3 and 4) for plates 1 and 2. The governing differential equations for each element are solved separately. At the ends of each element the appropriate boundary conditions are satisfied.

In a double-lap joint, because of symmetry about the x-axis, the lateral deflections of the joint are small compared with the joint thickness and, therefore, there is no need to consider the effects of large deflections in the analysis. The overhang regions are treated as unbonded elements. At the support ends of the overhang (C and D) support conditions are satisfied and at the junctions of overhangs and lap region (A and B) interface conditions are satisfied.

In a single-lap joint, the deflections can be of the order of the joint thickness, depending on the overall length of the joint and the applied load. Therefore, the effect of large deflections should be taken into account in the analysis. This is done approximately by carrying out the analysis in two stages: (1) the forces and displacements at the two ends of the lap region (A and B) are obtained by accounting for large deflections in an approximate way (see appendix A) and (2) the forces and displacements thus obtained are imposed on the lap region at the junctions A and B.

A flush joint, in which the overhang region 2 is very small, is analyzed much like a single-lap joint except that the boundary conditions at D are different for the two cases (see appendix A).

## GOVERNING DIFFERENTIAL EQUATIONS

### Bonded Elements

The governing differential equations were derived for the  $n$ th element. However, in equations (1) to (23) the index  $n$  is dropped for the sake of simplicity. In this derivation, the joints are assumed to be in a state of either plane stress or plane strain in the  $xz$ -plane. A unit width is chosen.

The displacements  $u$  and  $w$  in each plate are expanded in terms of polynomials in the  $z$ -direction; the coefficients of these polynomials are functions of  $x$  only. Enough terms are retained in the expansion to obtain a good approximation of the transverse shear stress  $\sigma_{xz}$  and transverse normal stress  $\sigma_z$  in the plates. For double-lap joints, symmetry about the  $x$ -axis is taken into account in the expressions for plate 1, and only the portion  $z \geq 0$  is considered. The expressions for displacements follow.

For single-lap and flush joints:

$$\left. \begin{aligned} u(j) &= t^* \sum_{i=0}^2 \phi(j,i) Z^i \\ w(j) &= t^* \sum_{i=0}^2 \psi(j,i) Z^i \end{aligned} \right\} \quad (j = 1, 2) \quad (1)$$

In the thin-beam analysis,

$$\left. \begin{aligned} \phi(j,2) &= \psi(j,1) = \psi(j,2) = 0 \\ \phi(j,1) &= \frac{-\partial \psi(j,0)}{\partial x} \end{aligned} \right\} \quad (j = 1, 2)$$

For double-lap joints:

$$\left. \begin{aligned} u(1) &= t^* \sum_{i=0}^1 \phi(1,i) Z^{2i} \\ w(1) &= t^* \sum_{i=0}^1 \psi(1,i) Z^{2i+1} \end{aligned} \right\} \quad (2)$$

and  $u(2)$  and  $w(2)$  are given by equations (1). In the thin-beam analysis,

$$\phi(1,1) = \psi(1,0) = \psi(1,1) = \phi(2,2) = \psi(2,1) = \psi(2,2) = 0$$

$$\phi(2,1) = \frac{\partial \psi(2,0)}{\partial x}$$

In equations (1) and (2)  $\phi$  and  $\psi$  are functions of  $x$  only.

Strains are obtained by differentiating equations (1) for single-lap and flush joints to give

$$\left. \begin{aligned} \epsilon_x(j) &= \sum_{i=0}^2 \phi'(j,i)Z^i \\ \epsilon_z(j) &= \sum_{i=0}^2 \psi(j,i)Z^{i-1} \\ \epsilon_{xz}(j) &= \sum_{i=0}^2 \left[ \phi(j,i)Z^{i-1} + \psi'(j,i)Z^i \right] \end{aligned} \right\} \quad (j = 1,2) \quad (3)$$

and by differentiating equations (2) for double-lap joints to give

$$\left. \begin{aligned} \epsilon_x(1) &= \sum_{i=0}^1 \phi'(1,i)Z^{2i} \\ \epsilon_z(1) &= \sum_{i=0}^1 (2i + 1)\psi(1,i)Z^{2i} \\ \epsilon_{xz}(1) &= \sum_{i=0}^1 2i\phi(1,i)Z^{2i-1} + \psi'(1,i)Z^{2i+1} \end{aligned} \right\} \quad (4)$$

and

$\epsilon_x(2)$ ,  $\epsilon_z(2)$ , and  $\epsilon_{xz}(2)$  are given by equations (3).

The stress-strain relations for plane stress or plane strain are given by

$$\begin{bmatrix} \sigma_x(j) \\ \sigma_z(j) \\ \sigma_{xz}(j) \end{bmatrix} = \begin{bmatrix} C_{11}(j) & C_{12}(j) & 0 \\ C_{12}(j) & C_{22}(j) & 0 \\ 0 & 0 & C_{33}(j) \end{bmatrix} \begin{bmatrix} \epsilon_x(j) \\ \epsilon_z(j) \\ \epsilon_{xz}(j) \end{bmatrix} \quad (5)$$

Substitution of equations (3) and (4) into equation (5) yields the following expressions for stresses in terms of displacements.

For single-lap and flush joints:

$$\left. \begin{aligned} \sigma_x(j) &= \sum_{i=0}^2 \left[ C_{11}(j) \phi'(j,i) Z^i + C_{12}(j) \psi(j,i) Z^{i-1} \right] \\ \sigma_z(j) &= \sum_{i=0}^2 \left[ C_{12}(j) \phi'(j,i) Z^i + C_{22}(j) \psi'(j,i) Z^{i-1} \right] \\ \sigma_{xz}(j) &= \sum_{i=0}^2 C_{33}(j) \left[ \phi(j,i) Z^{i-1} + \psi'(j,i) Z^i \right] \end{aligned} \right\} \quad (j = 1, 2) \quad (6)$$

For double-lap joints:

$$\left. \begin{aligned} \sigma_x(1) &= \sum_{i=0}^1 \left[ C_{11}(1) \phi'(1,i) Z^{2i} + C_{12}(1) \psi(1,i) (2i + 1) Z^{2i} \right] \\ \sigma_z(1) &= \sum_{i=0}^1 \left[ C_{12}(1) \phi'(1,i) Z^{2i} + C_{22}(1) \psi(1,i) (2i + 1) Z^{2i} \right] \\ \sigma_{xz}(1) &= \sum_{i=0}^1 C_{33}(1) \left[ 2i \phi(1,i) Z^{2i-1} + \psi'(1,i) Z^{2i+1} \right] \end{aligned} \right\} \quad (7)$$

and  $\sigma_x(2)$ ,  $\sigma_z(2)$ , and  $\sigma_{xz}(2)$  are given by equations (6).

The adhesive layer at the bond surface is represented by equivalent linear springs in the x- and z-directions. The spring constants  $k_x^*$  and  $k_z^*$  are given by the equations

$$k_x^* = \frac{G_g^*}{\eta^*} \quad k_z^* = \frac{E_g^*}{\eta^*} \quad (8)$$

Thus, the shear stress  $\tau$  and the transverse normal stress  $\sigma$  in the bond are given by

$$\left. \begin{aligned} \tau &= k_x^* [u(2) - u(1)]_{Z=1} \\ \sigma &= k_z^* [w(2) - w(1)]_{Z=1} \end{aligned} \right\} \quad (9)$$

Substituting equations (1) and (2) into equations (9) yields

For single-lap and flush joints:

$$\left. \begin{aligned} \tau &= k_x \sum_{i=0}^2 [\phi(2,i) - \phi(1,i)] \\ \sigma &= k_z \sum_{i=0}^2 [\psi(2,i) - \psi(1,i)] \end{aligned} \right\} \quad (10)$$

For double-lap joints:

$$\left. \begin{aligned} \tau &= k_x \left[ \sum_{i=0}^2 \phi(2,i) - \sum_{i=0}^1 \phi(1,i) \right] \\ \sigma &= k_z \left[ \sum_{i=1}^3 \psi(2,i) - \sum_{i=0}^1 \psi(1,i) \right] \end{aligned} \right\} \quad (11)$$

The equations of equilibrium of two-dimensional linear elasticity are

$$\left. \begin{aligned} \frac{\partial \sigma_x(j)}{\partial x} + \frac{\partial \sigma_{xz}(j)}{\partial z} &= 0 \\ \frac{\partial \sigma_{xz}(j)}{\partial x} + \frac{\partial \sigma_z(j)}{\partial z} &= 0 \end{aligned} \right\} \quad (j = 1, 2) \quad (12)$$

The equilibrium conditions at the bond surface are

$$\left. \begin{aligned} \sigma_{xz}(1) = \sigma_{xz}(2) = \tau \\ \sigma_z(1) = \sigma_z(2) = \sigma \end{aligned} \right\} \quad (13)$$

The stress-free conditions on the outer surfaces are

$$\left. \begin{aligned} \sigma_{xz}(1) = \sigma_z(1) = 0 & \quad (Z = 1 - c \text{ for single-lap joints}) \\ \sigma_{xz}(1) = \sigma_z(1) = 0 & \quad (Z = 0 \text{ for flush joints}) \\ \sigma_{xz}(2) = \sigma_z(2) = 0 & \quad (Z = 1 + h \text{ for all joints}) \end{aligned} \right\} \quad (14)$$

Equations (12) are multiplied by  $Z^k$  and integrated by parts through the thickness for each plate. During integration the equilibrium conditions at the bond surface (eqs. (13)) and stress-free conditions at the outer surfaces (eqs. (14)) are satisfied. This process yields

$$N'(j,k) - kQ(j,k-1) - (-1)^j \tau = 0 \quad (15a)$$

$$Q'(j,k) - kV(j,k-1) - (-1)^j \sigma = 0 \quad (15b)$$

The values of  $k$  in equations (15a) and (15b) are the same as the powers of  $Z$  used in the expansions of  $u$  and  $w$ , respectively (see eqs. (1) and (2)). That is, for single-lap and flush joints:  $k = 0, 1, 2$  for both equations (15a) and (15b); for double-lap joints:  $k = 0, 2$  for equation (15a) and  $k = 1, 3$  for equation (15b).

In equations (15),  $N$ ,  $Q$ , and  $V$  are integrals of stress given by

$$\left\{ N(j,k); V(j,k); Q(j,k) \right\} = \int_{\alpha(j)}^{\beta(j)} \left\{ \sigma_x(j); \sigma_z(j); \sigma_{xz}(j) \right\} Z^k dZ \quad (16)$$

$$\left. \begin{aligned} \alpha(1) = 1 - c & \quad (\text{Single-lap joints}) \\ \alpha(1) = 0 & \quad (\text{Double-lap and flush joints}) \end{aligned} \right\} \quad (17a)$$

$$\alpha(2) = \beta(1) = 1 \quad \beta(2) = 1 + h \quad (17b)$$

Substituting equations (6) and (7) into equation (16), the integrals of stresses are obtained in terms of displacements and are written as follows.

For single-lap and flush joints:

$$\left. \begin{aligned} N(j,k) &= \sum_{i=0}^2 \left[ D_{11}(j,k+i) \phi'(j,i) + iD_{12}(j,k+i-1) \psi(j,i) \right] \\ V(j,k) &= \sum_{i=0}^2 \left[ D_{12}(j,k+i) \phi'(j,i) + iD_{22}(j,k+i-1) \psi(j,i) \right] \\ Q(j,k) &= \sum_{i=0}^2 \left[ iD_{33}(j,k+i-1) \phi(j,i) + D_{33}(j,k+i) \psi'(j,i) \right] \end{aligned} \right\} \quad (j = 1, 2) \quad (18)$$

For double-lap joints:

$$\left. \begin{aligned} N(1,k) &= \sum_{i=0}^1 \left[ D_{11}(1,k+2i) \phi'(1,i) + (2i + 1)D_{12}(1,k+2i) \psi(1,i) \right] \\ V(1,k) &= \sum_{i=0}^1 \left[ D_{12}(1,k+2i) \phi'(1,i) + (2i + 1)D_{22}(1,k+2i) \psi(1,i) \right] \\ Q(1,k) &= \sum_{i=0}^1 \left[ 2iD_{33}(1,k+2i-1) \phi(1,i) + D_{33}(1,k+2i+1) \psi'(1,i) \right] \end{aligned} \right\} \quad (19)$$

and  $N(2,k)$ ,  $V(2,k)$ , and  $Q(2,k)$  are given by equations (18).

In equations (18) and (19)

$$\left\{ D_{11}(j,g); D_{12}(j,g); D_{22}(j,g); D_{33}(j,g) \right\} = \int_{\alpha(j)}^{\beta(j)} \left\{ C_{11}(j); C_{12}(j); C_{22}(j); C_{33}(j) \right\} Z^g dZ \quad (20)$$

when  $g$  is a dummy variable and  $\alpha$  and  $\beta$  are obtained from equations (17). If the material properties are constant through the thickness, equation (20) becomes

$$\left\{ D_{11}(j,g); \dots \right\} = \left\{ C_{11}(j,g); \dots \right\} \frac{\beta(j)^{g+1} - \alpha(j)^{g+1}}{g+1} \quad (21)$$

Substituting equations (18) and (19) into equations (15) yields the following governing differential equations.

For single-lap and flush joints:

$$\begin{aligned} & \sum_{i=0}^2 \left\{ D_{11}(j,k+i) \phi''(j,i) - kiD_{33}(j,k+i-2) \phi(j,i) \right. \\ & \left. + \left[ iD_{12}(j,k+i-1) - kD_{33}(j,k+i-1) \right] \psi'(j,i) \right\} \\ & - (-1)^j k_x \sum_{i=0}^2 \left[ \phi(2,i) - \phi(1,i) \right] = 0 \end{aligned} \quad (22a)$$

$$\begin{aligned} & \sum_{i=0}^2 \left\{ \left[ iD_{33}(j,k+i-1) - kD_{12}(j,k+i-1) \right] \phi'(j,i) \right. \\ & \left. + D_{33}(j,k+i) \psi''(j,i) - kiD_{22}(j,k+i-2) \psi(j,i) \right\} \\ & - (-1)^j k_z \sum_{i=0}^2 \left[ \psi(2,i) - \psi(1,i) \right] = 0 \end{aligned} \quad (22b)$$

For equations (22a) and (22b)  $j = 1, 2$  and  $k = 0, 1, 2$ .

For double-lap joints:

$$\begin{aligned}
& \sum_{i=0}^1 \left\{ D_{11}(1, k+2i) \phi''(1, i) - 2kiD_{33}(1, k+2i-2) \phi(1, i) \right. \\
& \left. + \left[ (2i+1)D_{12}(1, k+2i) - kD_{33}(1, k+2i) \right] \psi'(1, i) \right\} \\
& + k_x \left[ \sum_{i=0}^2 \phi(2, i) - \sum_{i=0}^1 \phi(1, i) \right] = 0 \tag{23a}
\end{aligned}$$

$$\begin{aligned}
& \sum_{i=0}^1 \left\{ \left[ 2iD_{33}(1, k+2i-1) - kD_{12}(1, k+2i-1) \right] \phi'(1, i) \right. \\
& \left. + D_{33}(1, k+2i+1) \psi''(1, i) - k(2i+1)D_{22}(1, k+2i-1) \psi(1, i) \right\} \\
& + k_z \left[ \sum_{i=0}^2 \psi(2, i) - \sum_{i=0}^1 \psi(1, i) \right] = 0 \tag{23b}
\end{aligned}$$

$$\begin{aligned}
& \sum_{i=0}^2 \left\{ D_{11}(2, k+i) \phi''(2, i) - kiD_{33}(2, k+i-2) \phi(2, i) \right. \\
& \left. + \left[ iD_{12}(2, k+i-1) - kD_{33}(2, k+i-1) \right] \psi'(2, i) \right\} \\
& - k_x \left[ \sum_{i=0}^2 \phi(2, i) - \sum_{i=0}^1 \phi(1, i) \right] = 0 \tag{23c}
\end{aligned}$$

$$\begin{aligned}
& \sum_{i=0}^2 \left\{ \left[ iD_{33}(2,k+i-1) - kD_{12}(2,k+i-1) \right] \phi'(2,i) \right. \\
& \left. + D_{33}(2,k+i) \psi''(2,i) - kiD_{22}(2,k+i-2) \psi(2,i) \right\} \\
& - k_z \left[ \sum_{i=0}^2 \psi(2,i) - \sum_{i=0}^1 \psi(1,i) \right] = 0 \tag{23d}
\end{aligned}$$

For equation (23a),  $k = 0, 2$ ; for equation (23b),  $k = 1, 3$ ; and for equations (23c) and (23d),  $k = 0, 1, 2$ . Note that all the preceding equations were derived for the  $n$ th element but the index  $n$  was not included for the sake of simplicity. In the remainder of the paper, the index  $n$  is included (see appendix B). The procedure for solution of equations (22) and (23) is given in appendix C.

#### Unbonded Elements

For an unbonded element, the governing differential equations are the same as those for the corresponding plate in the bonded element, but with  $k_x$  and  $k_z$  equal to zero.

#### PROCEDURE FOR ANALYSIS

The following procedures were used in the analysis for the respective cases.

For single-lap and flush joints:

- (1) The differential equations (22) are solved for all the elements in the lap region (see appendix C).
- (2) The forces and displacements at the junctions (A and B) between the lap region and the overhangs are obtained with large deflections taken into account (see appendix A).
- (3) All the interface conditions within the lap region are satisfied. At junctions A and B the proper forces and displacements obtained in step 2 are imposed (see appendix B).
- (4) The resulting simultaneous algebraic equations are solved to obtain the arbitrary constants. Displacements and stresses in the plates and shear and peel stresses in the bond are calculated by using equations (1), (6), and (10).

For double-lap joints:

(1) The differential equations (23) are solved for all the elements in the lap region (see appendix C).

(2) The differential equations are solved for the overhang regions. (For overhang region 1, eqs. (23a) and (23b) with  $k_x = k_z = 0$ ; for overhang region 2, eqs. (23c) and (23d) with  $k_x = k_z = 0$ .)

(3) All the interface conditions within the lap region and at junctions A and B are satisfied (see appendix B).

(4) The boundary conditions at the supports are satisfied (see appendix B).

(5) The resulting simultaneous algebraic equations are solved to obtain the arbitrary constants. Displacements and stresses in the plates and shear and peel stresses in the bond are calculated using equations (2), (7), and (11).

## NUMERICAL RESULTS AND DISCUSSION

Numerical results are presented in figures 3 to 8 for single-lap, flush, and double-lap joints. In the examples of double-lap and flush joints, the two main plates which are being joined are of the same material and thickness. In all the examples, the plates are of unidirectional composite material. All elastic moduli are nondimensionalized by dividing by  $E_f^*(1)$ , the Young's modulus of the fiber in plate 1. All linear dimensions are nondimensionalized by dividing by  $t^*$ , the thickness of overhang 1 in single-lap and flush joints or the half-thickness of overhang 1 in double-lap joints. The nondimensional Young's modulus of the plate resin is 0.00776 in all examples. The nondimensional Young's and shear moduli of the adhesive in all examples, except those in figure 4, are 0.00867 and 0.00155, respectively. In figures 3 and 4, results from the refined analysis and thin-beam analysis (the analyses in refs. 1 and 2 were extended for the present configurations) are presented. In figures 5 to 8, only the results obtained from the refined analysis are presented. In single-lap and flush joints, the stresses and displacements are nonlinear with respect to the applied stress  $p$ , and the results are presented for a typical case of  $p/E_f^*(1) = 0.002$ .

The longitudinal distribution of the direct and shear stresses in the bond are plotted in figure 3 for two types of plate 2 fiber materials. In single-lap joints (figs. 1(a), 3(a), and 3(b)) and flush joints (figs. 1(b), 3(c), and 3(d)), the direct stress in the bond is tensile (i.e., peeling type) at both ends A and B. In double-lap joints (figs. 1(c), 3(e), and 3(f)), the direct stress in the bond is compressive at the inner end B, whereas it is tensile at the outer end A. Generally, both the maximum peel and shear stresses occur at the inner end B in flush joints (figs. 1(b), 3(c), and 3(d)). The maximum shear stress in double-lap

joints (figs. 1(c), 3(e), and 3(f)) and the maximum peel and shear stresses in single-lap joints (figs. 1(a), 3(a), and 3(b)) could occur at either end, depending on the relative thickness and elastic moduli of plates 1 and 2. In single-lap joints, the ratios of peel and shear stresses at B to peel and shear stresses at A are greater when the thickness or elastic moduli of plate 2 are smaller (compare figs. 3(a) and 3(b)). In double-lap joints, the ratio of the shear stress at B to shear stress at A is larger when the thickness or elastic moduli of the lap plates are smaller (compare figs. 3(e) and 3(f)).

For all joints, the maximum peel stress in the bond as a function of the adhesive shear modulus for various values of the adhesive Young's modulus is shown in figures 4(a), 4(c), and 4(e). The maximum shear stress in the bond as a function of the adhesive Young's modulus for various values of the adhesive shear modulus is shown in figures 4(b), 4(d), and 4(f). In all joints, the maximum peel stress in the bond is larger when the Young's modulus or the shear modulus of the adhesive is larger (figs. 4(a), 4(c), and 4(e)). Also, the maximum shear stress in the bond is larger when the shear modulus of the adhesive is larger but is not significantly influenced by the adhesive Young's modulus (see figs. 4(b), 4(d), and 4(f)). Thus, a reduction in adhesive shear modulus reduces both maximum peel and shear stresses in the bond, but a reduction in adhesive Young's modulus reduces only the peel stress.

The thin-beam and refined analyses give similar longitudinal distributions of shear and peel stresses in the bond (figs. 3(a) to 3(f)). Also, the thin-beam analysis yields reasonably accurate values of maximum peel stress in the bond at low values of adhesive shear and Young's moduli (figs. 4(a), 4(c), and 4(e)) and of maximum shear stress at low values of adhesive shear modulus (figs. 4(b), 4(d), and 4(f)). Although the results are not included, it was found that errors obtained by using thin-beam analysis are larger when lap length is smaller.

For all joints, the maximum peel and shear stresses in the bond as functions of adhesive thickness are shown in figures 5(a), 5(d), and 5(g) and figures 5(b), 5(e), and 5(h), respectively. Also, the flexibility of the joint (as measured by the axial displacement of plate 1 at outer end A) as a function of adhesive thickness is shown in figures 5(c), 5(f), and 5(i). In all the joints, for larger adhesive thickness, the maximum peel stress (figs. 5(a), 5(d), and 5(g)) and maximum shear stress (figs. 5(b), 5(e), and 5(h)) in the bond are smaller whereas the joint flexibility (figs. 5(c), 5(f), and 5(i)) is slightly larger. Of

the three types of joints considered, for a given total adhesive thickness and joint volume,<sup>1</sup> the maximum peel and shear stresses are lowest in double-lap joints and highest in flush joints. The following table gives the results for a total adhesive thickness of  $0.2t^*$ :

$$\text{Joint volume} = \begin{cases} l^*(h^* + t^*) & \text{for single-lap joints} \\ 2l^*(h^* + t^*) & \text{for flush joints} \\ 4l^*(h^* + t^*) & \text{for double-lap joints} \end{cases}$$

Type of joint	$\sigma/p$	$-\tau/p$	Flexibility
Double lap <sup>a</sup>	0.056	0.07	40.3
Single lap	.10	.08	46.8
Flush	.35	.173	32.8

<sup>a</sup>Two bonds and thus the total adhesive thickness is twice the thickness of a single bond.

In general, for flush joints, the maximum peel stress in the bond is much higher than the maximum shear stress (figs. 5(d) and 5(e)). For moderate adhesive thicknesses ( $\eta = 0.1$  to  $0.2$ ), the maximum peel stress is nearly equal to the maximum shear stress in single-lap joints (figs. 5(a) and 5(b)) and double-lap joints (figs. 5(g) and 5(h)). Thus, the maximum peel stress can be roughly estimated if the approximate value of maximum shear stress in the bond is known.

In figure 6, data for the flush and double-lap joints are shown as a function of maximum direct stress in the lap plate. The lap-plate thickness is shown in figures 6(a) and 6(d); the maximum peel stress is shown in figures 6(b) and 6(e); and the maximum shear stress is shown in figures 6(c) and 6(f). Lap plates with three different moduli are considered. In both flush and double-lap joints, the maximum direct stress in the lap plate, which occurs at the inner end B (fig. 1), is larger when the lap-plate thickness is smaller (figs. 6(a) and 6(d)). In flush joints, the maximum shear stress in the bond is larger when the maximum lap-plate stress is larger or the lap-plate modulus is smaller (fig. 6(c)). Similar behavior is observed for maximum peel stress in the lower ranges of maximum lap-plate stress (fig. 6(b)). In double-lap joints, the maximum peel stress (fig. 6(e)) and the shear stress (fig. 6(f)) in the bond at the outer end A are smaller when the maximum lap-plate stress is larger or the lap-plate modulus is smaller. For the same conditions, the shear stress at the inner end B is larger (see dashed curves in fig. 6(f)). Therefore, to reduce the maximum bond shear stress in double-lap joints, it is advantageous to use a high-modulus lap plate; the minimum lap-plate thickness is then governed by either the strength (maximum allowable stress) of the lap plate or the strength of the bond in shear.

The preceding discussion referred to joints in which the plates are of constant thickness and the same bond is used along the entire length of the joint. In the following discussion, variations from these conditions are considered. For all joints, the bond shear stress at a particular location is a function of the load that is transferred from one plate to another at that location. The load transfer is in turn a function of the stiffness of the plates and the adhesive. When the plates are of constant thickness and the same bond is used along the entire length of the joint, a large amount of the load is transferred near the end or ends. Making the bond more flexible in the high-load-transfer region than in other regions or tapering the plates might reduce the high load transfer. Such a reduction will lower the maximum shear and peel stresses in the bond.

For all joints, the effect of combining flexible and stiff bonds is illustrated in figures 7(a) to 7(f). The maximum peel stresses in the flexible and stiff bonds are shown in figures 7(a), 7(c), and 7(e) as functions of length of stiff bond  $l_s$ ; the maximum shear stresses are shown in figures 7(b), 7(d), and 7(f). For  $l_s/l$  near 1, the maximum peel stress in the flexible bond is less when it is used in combination with a stiff bond than when it is used alone (solid curves). Similarly, the maximum peel stress in the stiff bond is less when it is used in combination with a flexible bond than when it is used alone (dashed curves). The two preceding observations are true for maximum shear stress also. A small length of stiff bond does not reduce the peel and shear stresses in the flexible bond. As  $l_s/l$  approaches unity, the stresses in the stiff bond are larger and the stresses in the flexible bond are smaller. Therefore, depending on the particular joint and bond properties, optimum lengths of stiff and flexible bonds can be chosen to assure the lowest possible stresses in the bond.

The maximum peel stress in the bond as a function of taper ratio ( $H_e/H_b$ ) is shown in figures 8(a) and 8(c) for single-lap and double-lap joints, respectively. The maximum shear stress in the bond is shown in figures 8(b) and 8(d). In single-lap joints, for larger taper (i.e., smaller taper ratio), the maximum peel (fig. 8(a)) and shear (fig. 8(b)) stresses are smaller; the decrease in peel stress is more pronounced than the decrease in shear stress. In double-lap joints, for larger taper, the maximum peel (fig. 8(c)) and shear stress at the outer end A (fig. 8(d)) are smaller, whereas the shear stress at the inner end B (fig. 8(d)) is slightly larger. Therefore, in double-lap joints, the maximum shear stress cannot be reduced by tapering. Further, in double-lap joints, bond length does not have a significant influence on stresses in the bond, when it is greater than 40 times the half-thickness of the main plate. Although the results are not included, it was found that tapering is not effective in flush joints.

## CONCLUDING REMARKS

A refined elastic analysis of bonded joints which accounts for transverse shear deformation and transverse normal stress was developed to obtain the stresses and displacements in the plates and in the bond. Single-lap, flush, and double-lap joints were analyzed. This analysis showed that the thin-beam analysis, which neglects transverse shear deformation and transverse normal stress, is, in general, reasonably accurate for estimating maximum peel and shear stresses. But, when the lap length is small or the stiffnesses of the bond in the longitudinal and thickness directions are high, the errors in the stresses in the bond could be high.

Maximum peel and shear stresses in the bond can be reduced by the following methods: (1) In all joints, making the bond flexible either by increasing the adhesive thickness or decreasing the adhesive elastic moduli, (2) in all joints, by using a combination of flexible and stiff bonds with flexible bond in regions of high stresses in the bond and stiff bond in regions of low stresses, (3) in double-lap joints, by using thinner but higher modulus lap plates, (4) in flush joints, by using thicker and higher modulus lap plates, and (5) in single-lap and double-lap (only peel stress) joints, by tapering the plate or plates. Of the three types of joints analyzed, for a given total adhesive thickness and joint volume, the double-lap joint had the smallest maximum stresses in the bond and the flush joint had the highest.

Langley Research Center,

National Aeronautics and Space Administration,

Hampton, Va., February 13, 1975.

## APPENDIX A

### EFFECT OF LARGE DEFLECTIONS ON SINGLE-LAP AND FLUSH JOINTS

As mentioned in the section "Analysis," for single-lap and flush joints, the forces and deflections at the ends of the lap region are calculated, taking the effect of large deflections into account in an approximate way. The procedure followed is like one used by Goland and Reissner (ref. 2). The complete joint is treated as a beam with discontinuities in the neutral axis (see fig. 9) as well as bending stiffness. In the lap region, the two plates are assumed to be perfectly bonded throughout and to act like a compound beam. From geometry, the eccentricity in the neutral axis  $\mu^*(s)$  is given by

$$\mu^*(s) = e^*(s) + 1 - d^*(s) - e^*(m+2) \quad (A1)$$

where  $e^*(s)$  is the distance from the neutral axis of the compound beam to the top surface of the  $s$ th segment of plate 1. If the material properties are uniform across the depth of the individual plates, then from elementary strength of materials, the distance  $e^*(s)$  and the bending stiffness  $K^*(s)$  are given by

$$\left. \begin{aligned} e^*(s) &= t^* \left( \frac{E(1) d(s)^2 + E(2) \left\{ [f(s) + d(s)]^2 - d(s)^2 \right\}}{2[E(1) d(s) + E(2) f(s)]} \right) \\ K^*(s) &= \frac{t^{*3}}{3} \left( E(1) \left\{ [d(s) - e(s)]^3 + e(s)^3 \right\} + E(2) \left\{ [f(s) + d(s) - e(s)]^3 - [d(s) - e(s)]^3 \right\} \right) \end{aligned} \right\} \quad (A2)$$

where

$$E(j) = C_{11}(j) + \frac{C_{12}(j)^2}{C_{22}(j)}$$

The support conditions at end C (fig. 9) are

$$M(m+2) = 0 \quad (A3a)$$

and

$$\zeta(m+2) = 0 \quad (A3b)$$

where  $M$  is the bending moment and  $\zeta$  is the nondimensional deflection.

## APPENDIX A

The boundary conditions at end D (fig. 9) are

For single-lap joints:

$$\text{Bending moment} \quad M(1) = 0 \quad (\text{A4a})$$

$$\text{Deflection} \quad \zeta(1) = 0 \quad (\text{A4b})$$

For flush joints:

$$\text{Shear force} \quad S(1) = 0 \quad (\text{A5a})$$

$$\text{Slope} \quad \frac{d\zeta(1)}{d\xi} = 0 \quad (\text{A5b})$$

The vertical reaction  $R$  at end C (fig. 9) is given by

$$\left. \begin{aligned} R &= \frac{P\mu(1)}{L} && \text{(Single-lap joints)} \\ R &= 0 && \text{(Flush joints)} \end{aligned} \right\} \quad (\text{A6})$$

The moment  $M(s)$  in the  $s$ th segment at location  $\xi$ , when the contribution of deflection is taken into account, is given by

$$M(s) = \left\{ R(L-\xi) - P[\mu(s) + \zeta(s)] \right\} t^* \quad (\text{A7})$$

According to thin-beam theory,

$$M(s) = -\frac{K^*(s)}{t^*} \frac{d^2\zeta(s)}{d\xi^2} \quad (\text{A8})$$

Therefore, from equations (A7) and (A8) after some manipulation

$$\frac{1}{g(s)^2} \frac{d^2\zeta(s)}{d\xi^2} - \zeta(s) = \mu(s) - \frac{R}{P}(L-\xi) \quad (\text{A9})$$

## APPENDIX A

where  $g(s) = t^* \sqrt{\frac{P}{K^*(s)}}$ . Solution of equation (A9) gives

$$\zeta(s) = \Upsilon(s) e^{g(s)\xi} + \Xi(s) e^{-g(s)\xi} - \mu(s) + \frac{R}{P}(L-\xi) \quad (\text{A10})$$

where  $\Upsilon(s)$  and  $\Xi(s)$  are arbitrary constants.

The conditions of continuity of displacements and slopes are satisfied at the ends of each segment. For the end segment 1 at D, either condition (A4b) or condition (A5b) is satisfied. For end segment  $m + 2$  at C, condition (A3b) is satisfied. The resulting set of simultaneous algebraic equations is solved to obtain the arbitrary constants.

Using equations (A10) and (A7) yields the deflections and moments at the end of the lap region.

## APPENDIX B

### BOUNDARY CONDITIONS

The equations for the boundary conditions are presented in this appendix.

For single-lap and flush joints:

(1) At interfaces  $X = a(n)$ , where  $n = 1, 2, \dots, r - 1$  (see fig. 2):

$$\left. \begin{aligned} N(n,j,k) &= N(n+1,j,k) \\ Q(n,j,k) &= Q(n+1,j,k) \\ \phi(n,j,k) &= \phi(n+1,j,k) \\ \psi(n,j,k) &= \psi(n+1,j,k) \end{aligned} \right\} \quad (j = 1, 2; \quad k = 0, 1, 2)$$

(2) At junction B,  $X = 0$ :

At the center line  $u(2)$  (see eqs. (1)) is expressed as

$$u(2) = \phi(1,2,0) + \phi(1,2,1) \left[ \frac{1+h(2)}{2} \right] + \phi(1,2,2) \left[ \frac{1+h(2)}{2} \right]^2 = 0$$

The direct stresses in the overhang were assumed to be linear across the thickness (see figs. 2 and 9)

$$\left. \begin{aligned} N(1,2,1) &= \left[ \frac{M(2)}{t^*} \right] + \frac{p[h(1)-1]}{2} \\ N(1,2,2) &= \left[ \frac{M(2)}{t^*} \right] [h(1)-1] + \frac{p[h(1)-1]^2}{3} \end{aligned} \right\} \quad (B1)$$

$$\psi(1,2,1) = \zeta(2) \quad (B2)$$

$$\psi(1,2,1) = \psi(1,2,2) = 0$$

$$N(1,1,k) = Q(1,1,k) = 0 \quad (k = 0, 1, 2)$$

## APPENDIX B

In equations (B1) and (B2),  $M(2)$  and  $\zeta(2)$  are moment and deflection at junction B (see figs. 2 and 9) for step 1 (which is same as segment 2) and are obtained by taking large deflections into account (see appendix A).

(3) At junction A (see figs. 2 and 9),  $X = a(r)$ :

$$N(r,1,0) = p$$

$$N(r,1,1) = M(m+1) + \frac{p}{2}$$

$$N(r,1,2) = M(m+1) + \frac{p}{3}$$

$$\psi(r,1,0) = \zeta(m+1)$$

$$\psi(r,1,1) = \psi(r,1,2) = 0$$

$$N(r,2,k) = Q(r,2,k) = 0 \quad (k = 0, 1, 2)$$

where  $M(m+1)$  and  $\zeta(m+1)$  are moment and deflection at junction A for step  $m$  (which is same as segment  $m + 1$ ) and are obtained by taking large deflections into account (see appendix A).

For double-lap joints:

(1) At interfaces,  $X = a(n)$ , where  $n = 1, 2, \dots, r - 1$  (see fig. 2):

$$N(n,1,k) = N(n+1,1,k) \quad (k = 0, 2)$$

$$Q(n,1,k) = Q(n+1,1,k) \quad (k = 1, 3)$$

$$\left. \begin{aligned} \phi(n,1,k) &= \phi(n+1,1,k) \\ \psi(n,1,k) &= \psi(n+1,1,k) \end{aligned} \right\} \quad (k = 0, 1)$$

$$\left. \begin{aligned} N(n,2,k) &= N(n+1,2,k) \\ Q(n,2,k) &= Q(n+1,2,k) \end{aligned} \right\} \quad (k = 0, 1, 2)$$

APPENDIX B

$$\left. \begin{aligned} \phi(n,2,k) &= \phi(n+1,2,k) \\ \psi(n,2,k) &= \psi(n+1,2,k) \end{aligned} \right\} \quad (k = 0, 1, 2)$$

(2) At junction B,  $X = 0$  (see fig. 2):

$$N(1,i,k) = 0 \quad (k = 0, 2)$$

$$Q(1,1,k) = 0 \quad (k = 1, 3)$$

$$\left. \begin{aligned} N(1,2,k) &= \hat{N}(1,k) \\ Q(1,2,k) &= \hat{Q}(1,k) \\ \phi(1,2,k) &= \hat{\phi}(1,k) \\ \psi(1,2,k) &= \hat{\psi}(1,k) \end{aligned} \right\} \quad (k = 0, 1, 2)$$

where  $\hat{\phi}$ ,  $\hat{\psi}$ ,  $\hat{N}_i$  and  $\hat{Q}$  refer to overhang 2.

(3) At junction A,  $X = a(r)$  (see fig. 2):

$$N(r,1,k) = \hat{N}(2,k) \quad (k = 0, 2)$$

$$Q(r,1,k) = \hat{Q}(2,k) \quad (k = 1, 3)$$

$$\left. \begin{aligned} \phi(r,1,k) &= \hat{\phi}(2,k) \\ \psi(r,1,k) &= \hat{\psi}(2,k) \end{aligned} \right\} \quad (k = 0, 1)$$

$$\left. \begin{aligned} N(r,2,k) &= 0 \\ Q(r,2,k) &= 0 \end{aligned} \right\} \quad (k = 0, 1, 2)$$

where  $\hat{\phi}$ ,  $\hat{\psi}$ ,  $\hat{N}$ , and  $\hat{Q}$  refer to overhang 1.

## APPENDIX B

- (4) At support D, where symmetry is assumed to be about a vertical axis through D (see figs. 1 and 2):

$$\left. \begin{array}{l} \hat{\phi}(2,k) = 0 \\ \hat{Q}(2,k) = 0 \end{array} \right\} \quad (k = 0, 1, 2)$$

where  $\hat{\phi}$  and  $\hat{Q}$  refer to overhang 2.

- (5) At support C, where the stress  $p$  is assumed to be uniform across the thickness (see figs. 1 and 2):

$$\hat{N}(1,0) = p$$

$$\hat{N}(1,2) = \frac{p}{3}$$

$$\hat{Q}(1,1) = \hat{Q}(1,3) = 0$$

where  $\hat{N}$  and  $\hat{Q}$  refer to overhang 1.

## APPENDIX C

### SOLUTION OF DIFFERENTIAL EQUATIONS (22) AND (23)

Equations (22) and (23) are simultaneous second-order ordinary differential equations. They can be formally written in matrix notation as

$$\left( [\Gamma] \frac{d^2}{dX^2} + [\Theta] \frac{d}{dX} + [\Pi] \right) \{X\} = \{0\} \quad (C1)$$

where  $[\Gamma]$ ,  $[\Theta]$ , and  $[\Pi]$  are coefficient matrices and  $\{X\}$  is a column matrix of  $\phi$  and  $\psi$ . Equation (C1) is solved by using any of the standard methods, such as the one described in reference 6. The solution of equation (C1) has the form

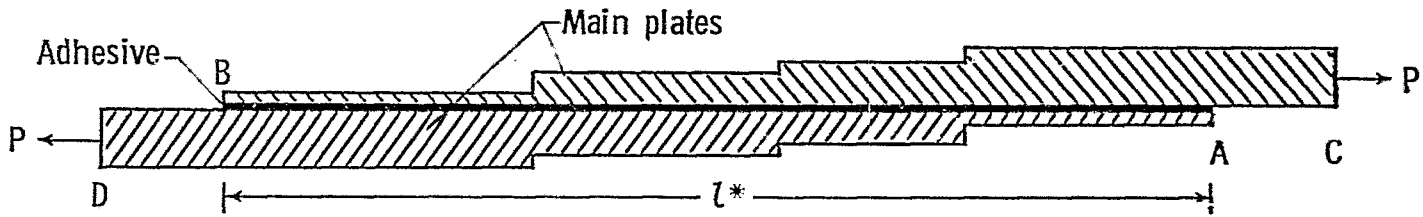
$$\{X\} = \sum_{\nu=1}^q F(\nu) \{A(\nu)\} \quad (C2)$$

where  $F(\nu)$  are arbitrary constants. The column matrices  $\{A(\nu)\}$  are constants or are power or exponential functions of  $X$ . The values of  $q$  are

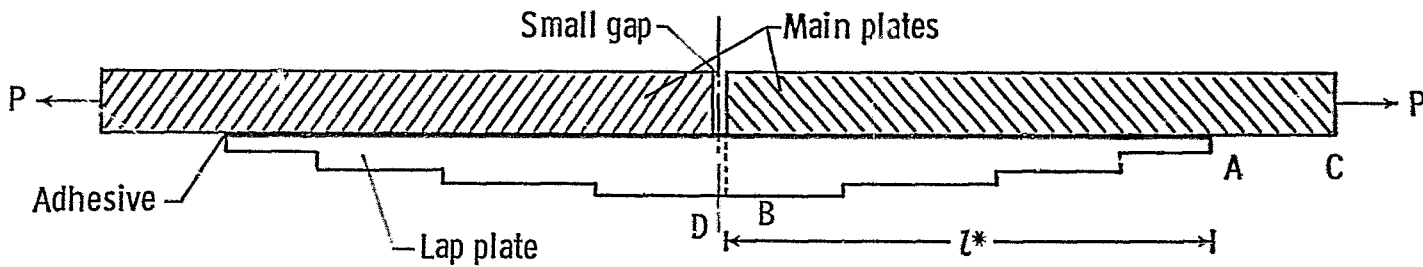
- 24 for single-lap and flush joints
- 20 for double-lap joints
- 12 for unbonded elements without symmetry about x-axis
- 8 for unbonded elements with symmetry about x-axis (plate 1 in double-lap joint)

## REFERENCES

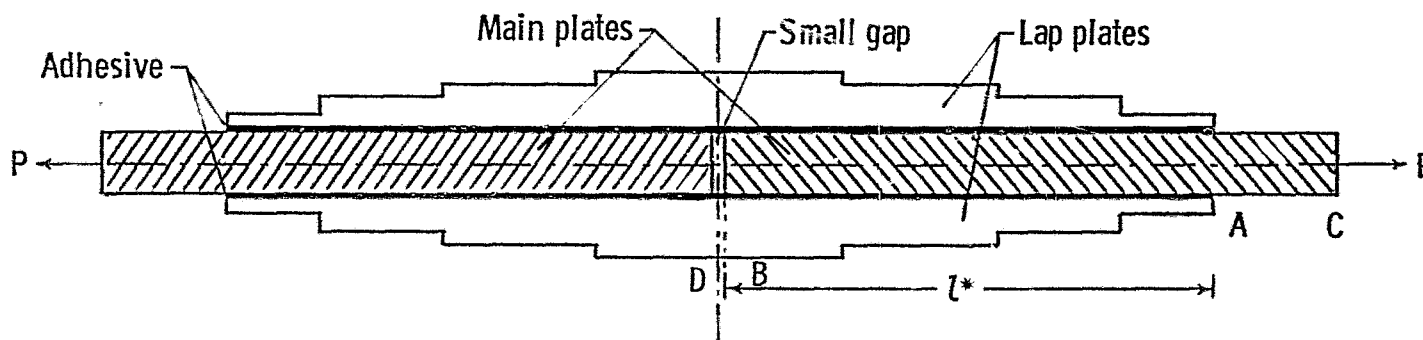
1. De Bruyne, N. A.: The Strength of Glued Joints. *Aircraft Eng.*, vol. XVI, no. 179, Apr. 1944, pp. 115-118.
2. Goland, M.; and Reissner, E.: The Stresses in Cemented Joints. *J. Appl. Mech.*, vol. 11, no. 1, Mar. 1944, pp. A-17 – A-27.
3. Erdogan, F.; and Ratwani, M.: Stress Distribution in Bonded Joints. *J. Compos. Mater.*, vol. 5, July 1971, pp. 378-393.
4. Wah, Thein: Stress Distribution in a Bonded Anisotropic Lap Joint. *Trans. ASME, Ser. H: J. Eng. Mater. & Technol.*, vol. 95, no. 3, July 1973, pp. 174-181.
5. Hart-Smith, L. J.: Analysis and Design of Advanced Composite Bonded Joints. NASA CR-2218, 1974.
6. Srinivas, S.: Analysis of Laminated, Composite, Circular Cylindrical Shells With General Boundary Conditions. NASA TR R-412, 1974.



(a) Single-lap joint.

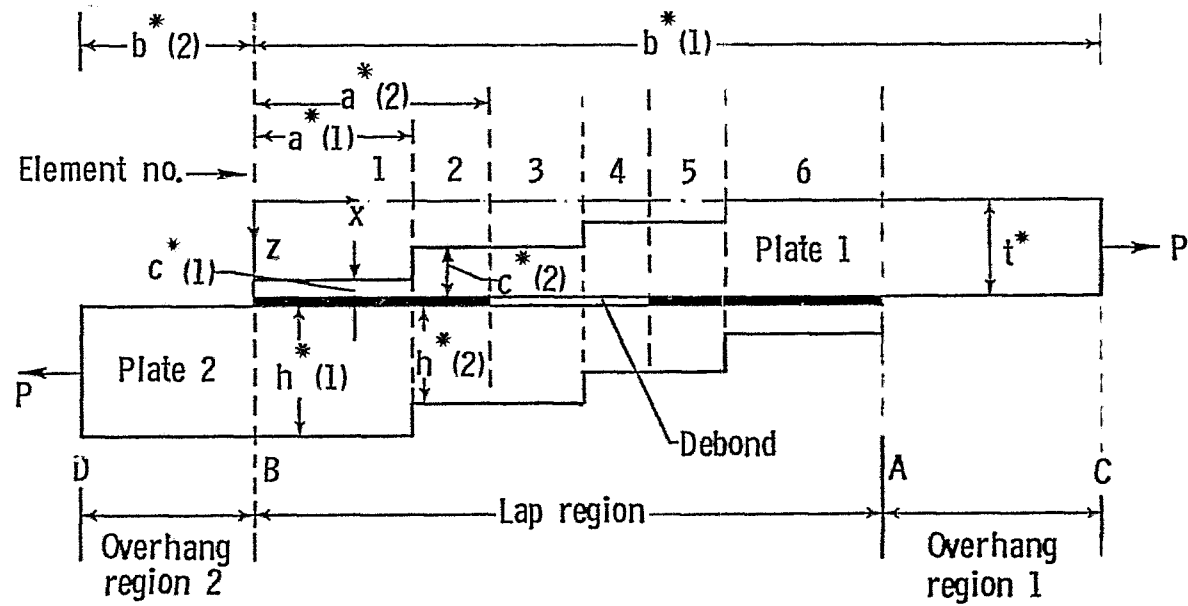


(b) Flush joint.



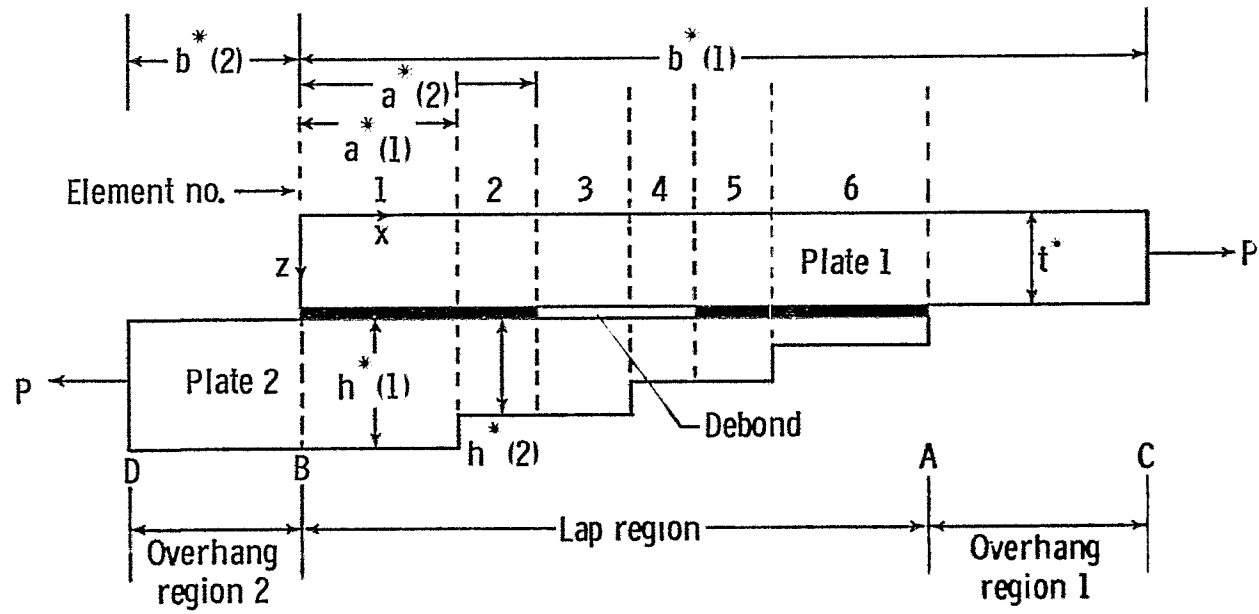
(c) Double-lap joint.

Figure 1.- Types of joints.



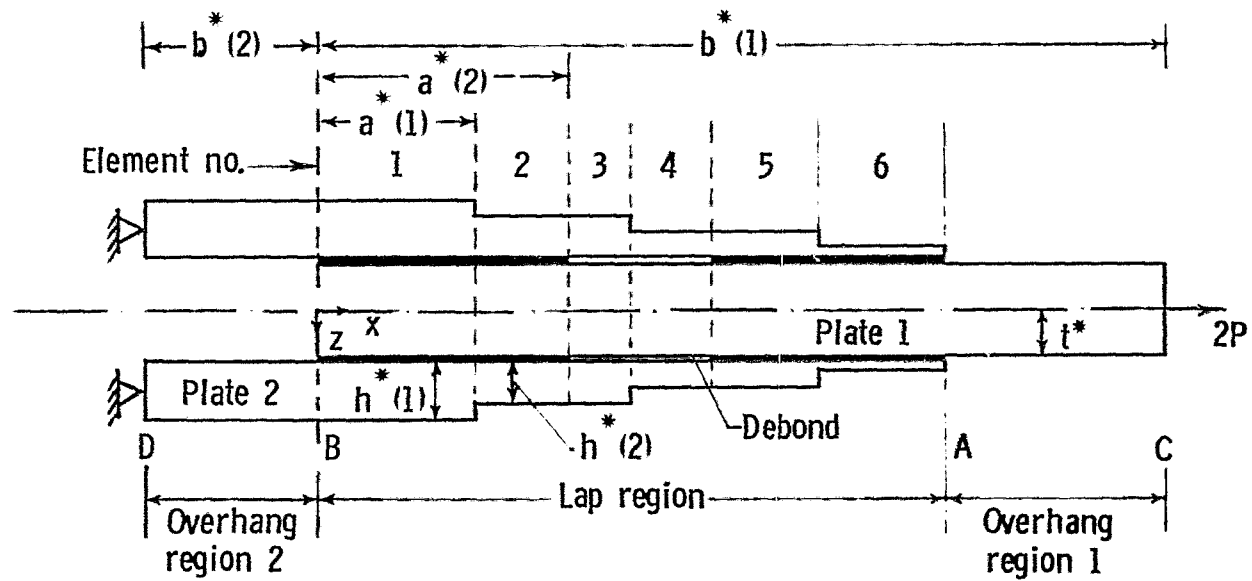
(a) Single-lap joint.

Figure 2.- Joint configuration (not to scale). (For illustration four steps are considered and bond between plates is assumed to have failed in elements 3 and 4. In this figure,  $m = 4$  and  $r = 6$ .)



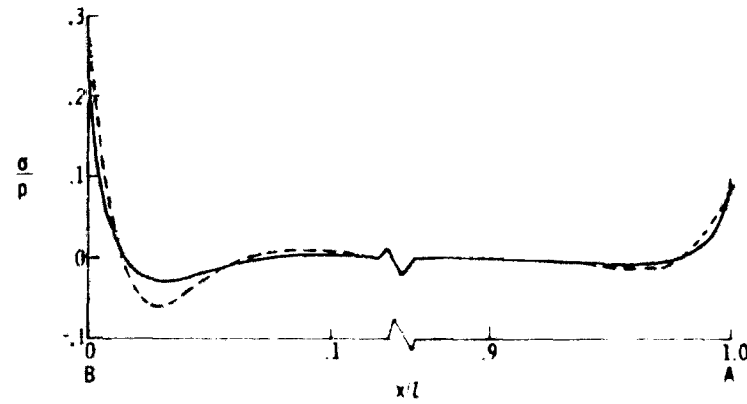
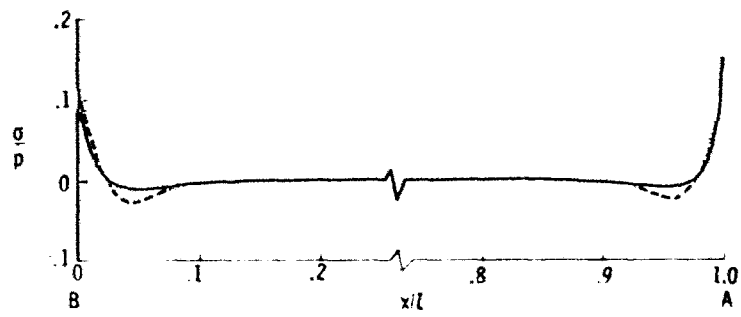
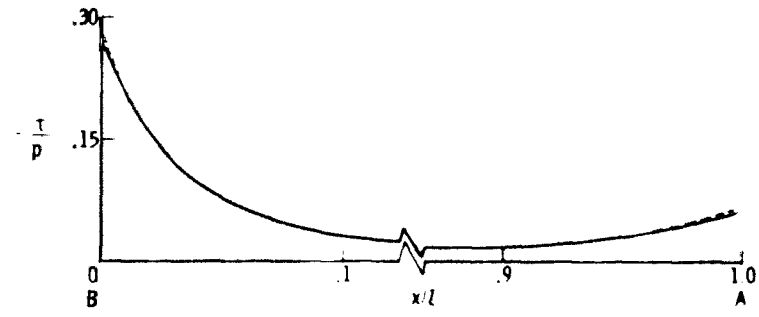
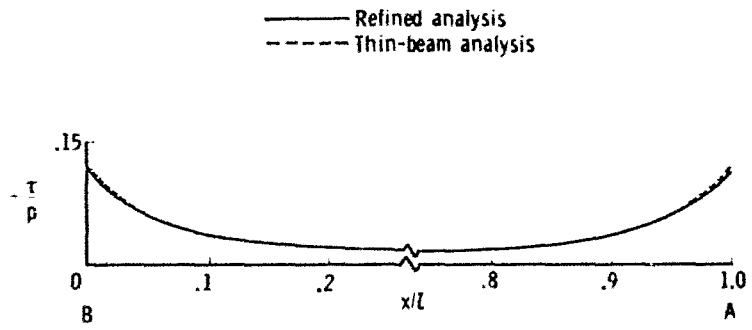
(b) Flush joint.

Figure 2.- Continued.



(c) Double-lap joint.

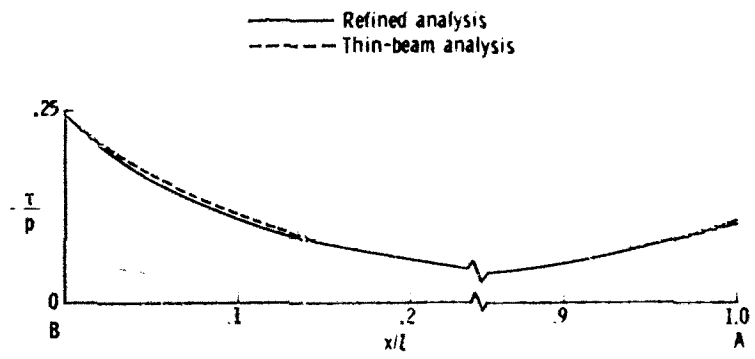
Figure 2.- Concluded.



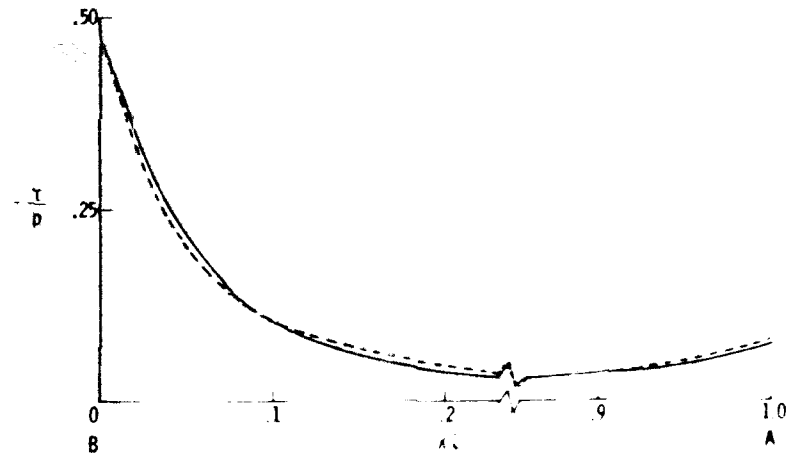
(a) Single-lap joint;  $l = 40$ ;  $\eta = 0.1$ ;  $\frac{E_f^*(2)}{E_f^*(1)} = 1$ .

(b) Single-lap joint;  $l = 40$ ;  $\eta = 0.1$ ;  $\frac{E_f^*(2)}{E_f^*(1)} = 0.207$ .

Figure 3.- Peel and shear stress distributions in bond. Plates are of same constant thickness.



(c) Flush joint;  $l = 20$ ;  $\eta = 0.1$ ;  $\frac{E_f^*(2)}{E_f^*(1)} = 1$ .



(d) Flush joint;  $l = 20$ ;  $\eta = 0.1$ ;  $\frac{E_f^*(2)}{E_f^*(1)} = 0.207$ .

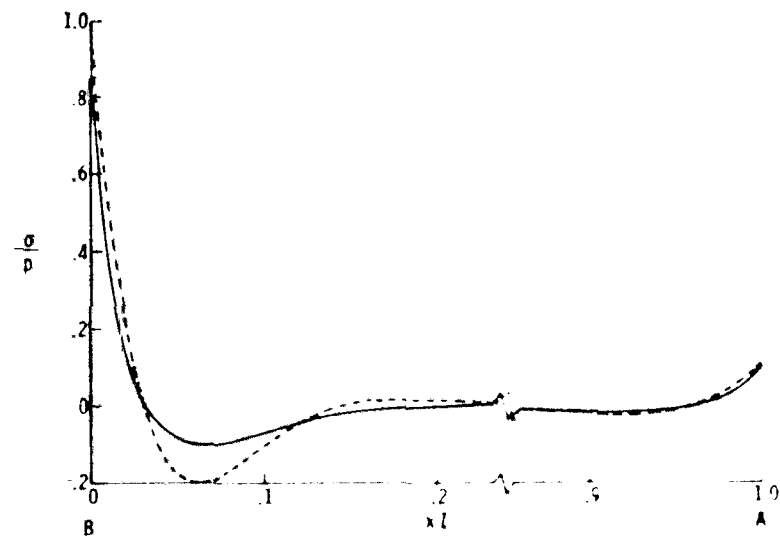
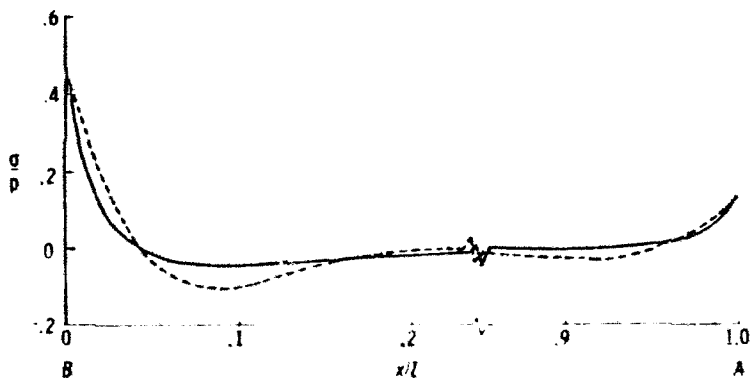
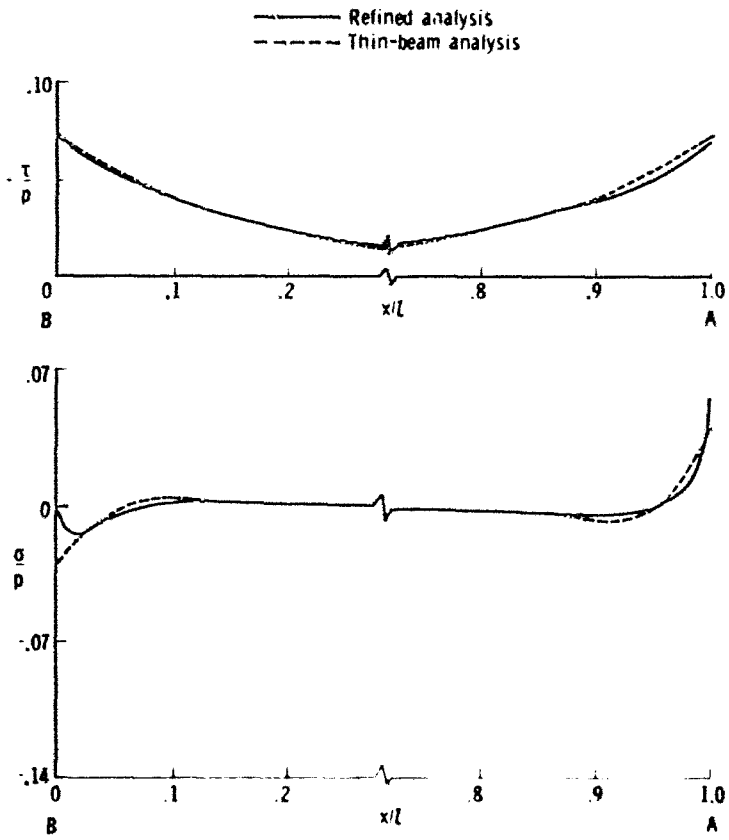
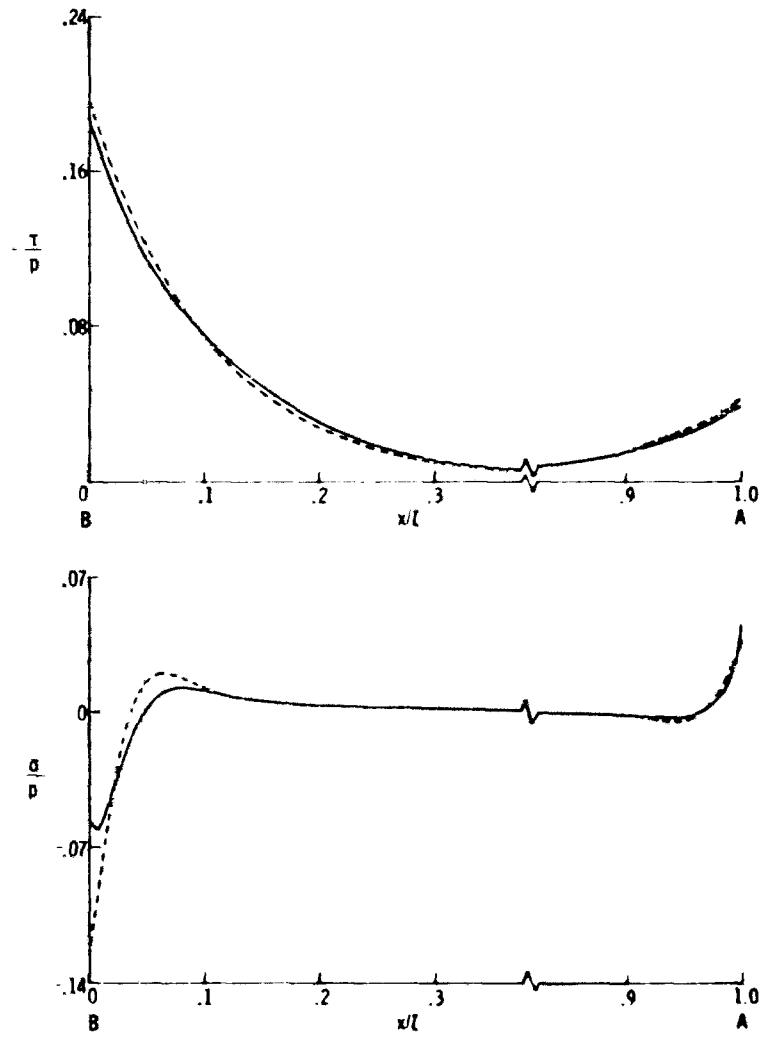


Figure 3.- Continued.

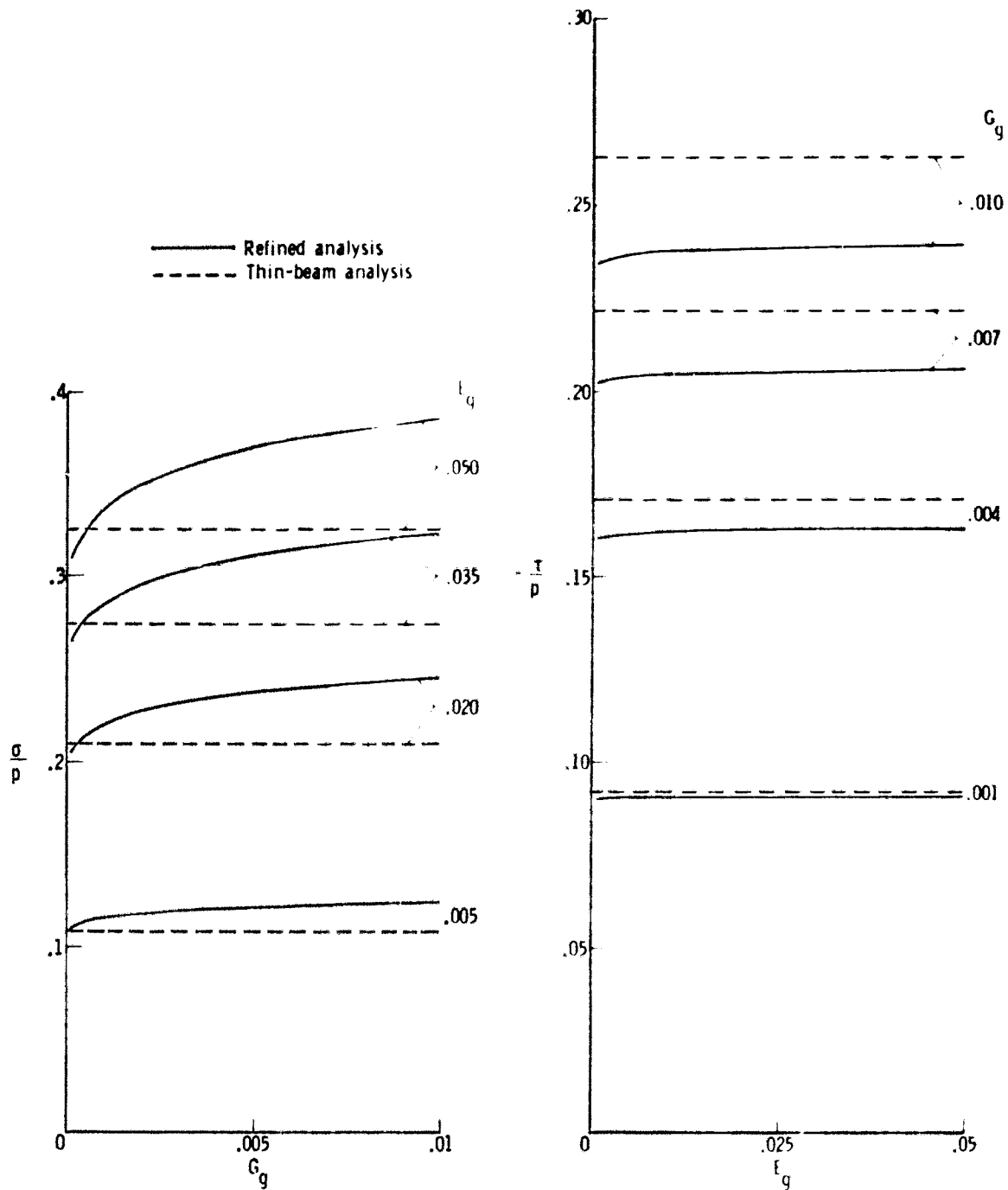


(e) Double-lap joint;  $l = 40$ ;  $\eta = 0.2$ ;  $\frac{E_f^*(2)}{E_f^*(1)} = 1$ .



(f) Double-lap joint;  $l = 40$ ;  $\eta = 0.2$ ;  $\frac{E_f^*(2)}{E_f^*(1)} = 0.207$ .

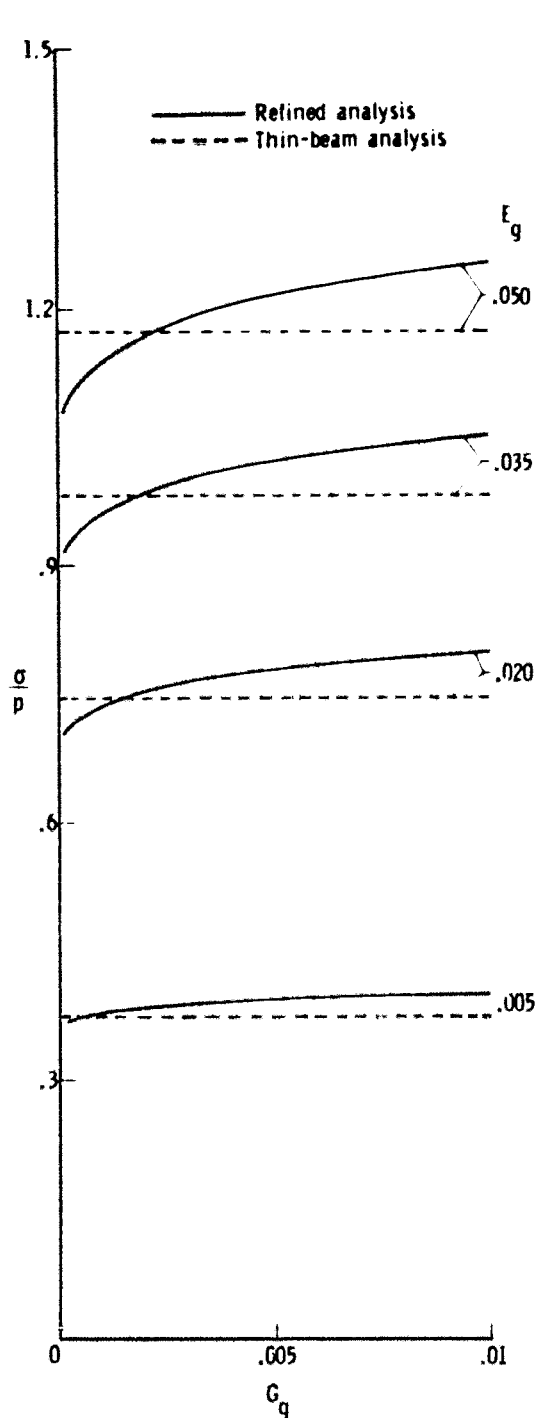
Figure 3.- Concluded.



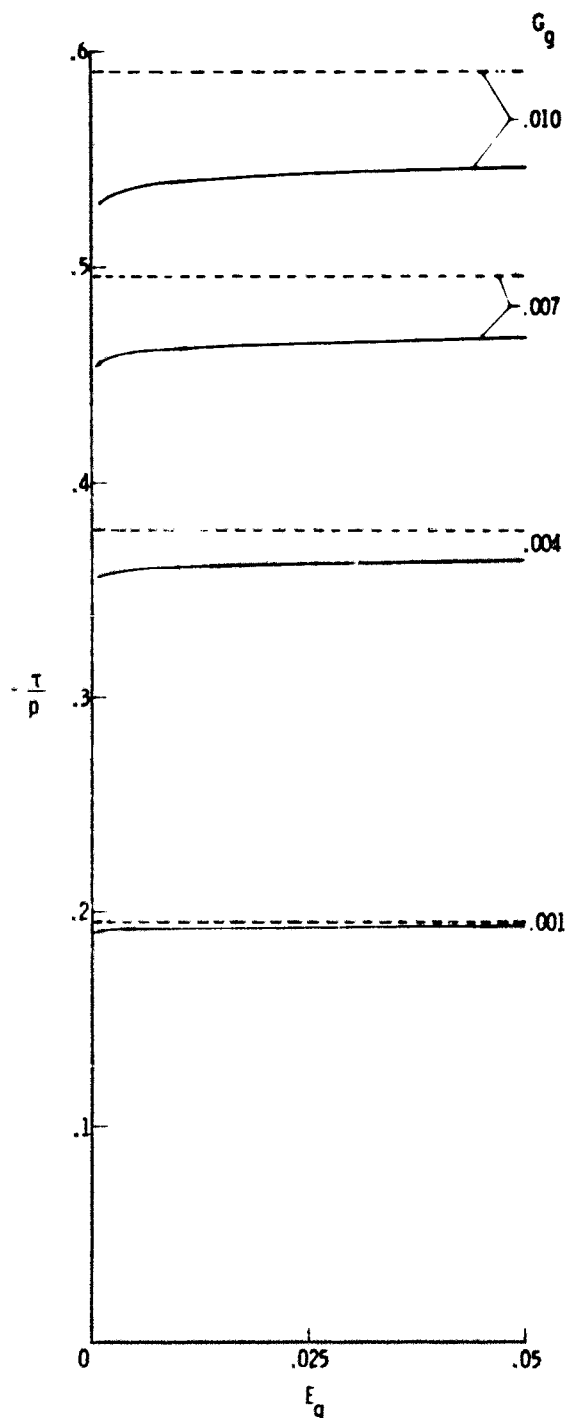
(a) Single-lap joint;  $l = 40$ ;  $\eta = 0.1$ ;  
 peel stress.

(b) Single-lap joint;  $l = 40$ ;  $\eta = 0.1$ ;  
 shear stress.

Figure 4.- Effect of adhesive moduli on maximum peel and shear stresses in bond.  
 Plates are of same material and same constant thickness.

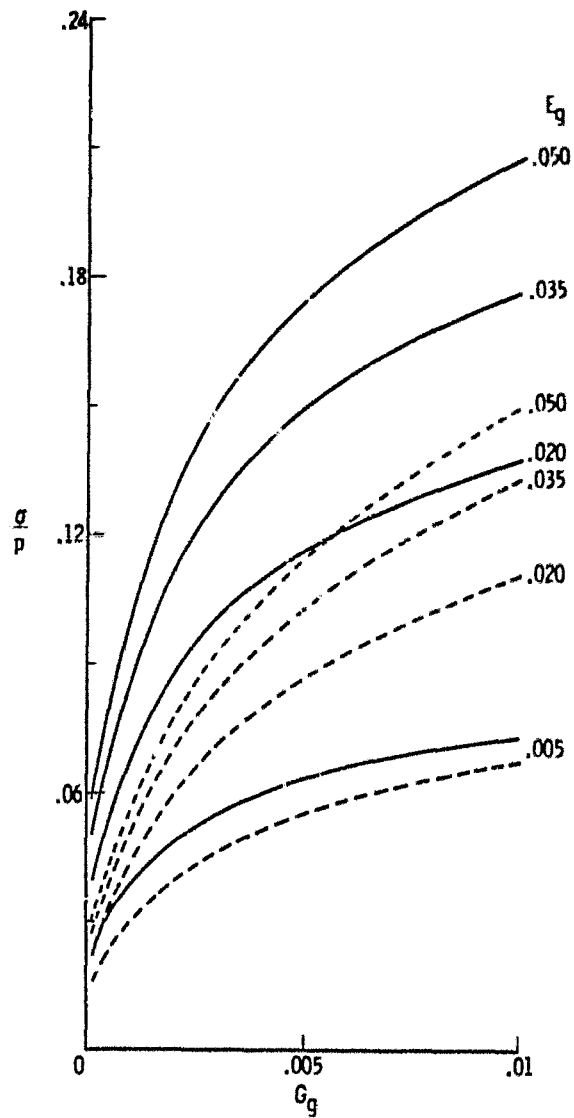


(c) Flush joint;  $l = 20$ ;  $\eta = 0.1$ ;  
peel stress.

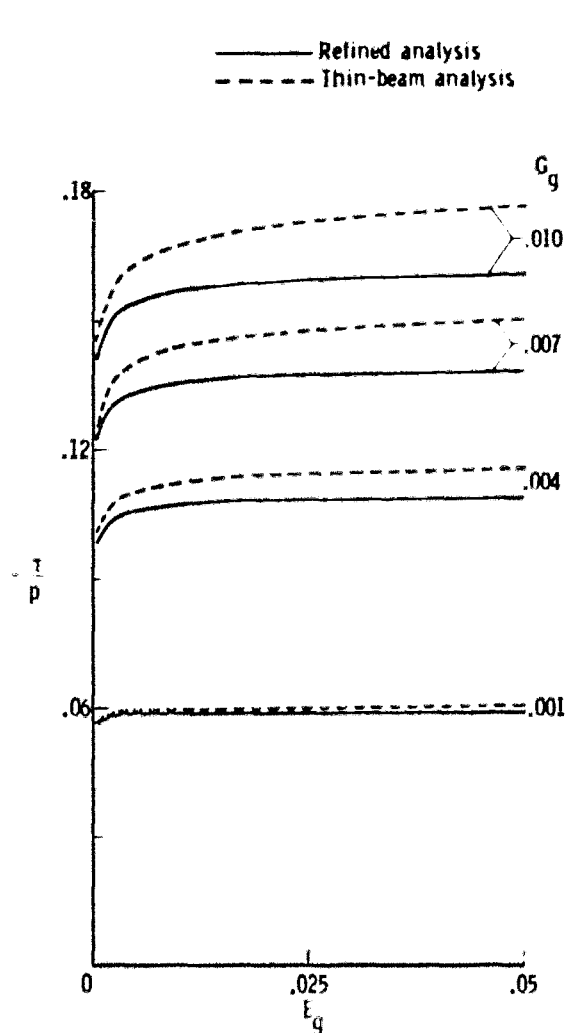


(d) Flush joint;  $l = 20$ ;  $\eta = 0.1$ ;  
shear stress.

Figure 4.- Continued.



(e) Double-lap joint;  $l = 40$ ;  $\eta = 0.2$ ;  
peel stress.



(f) Double-lap joint;  $l = 40$ ;  $\eta = 0.2$ ;  
shear stress. ( $\tau$  at outer end is  
plotted because maximum peel  
stress occurs there, although  $\tau$   
at inner end is slightly higher.)

Figure 4.- Concluded.

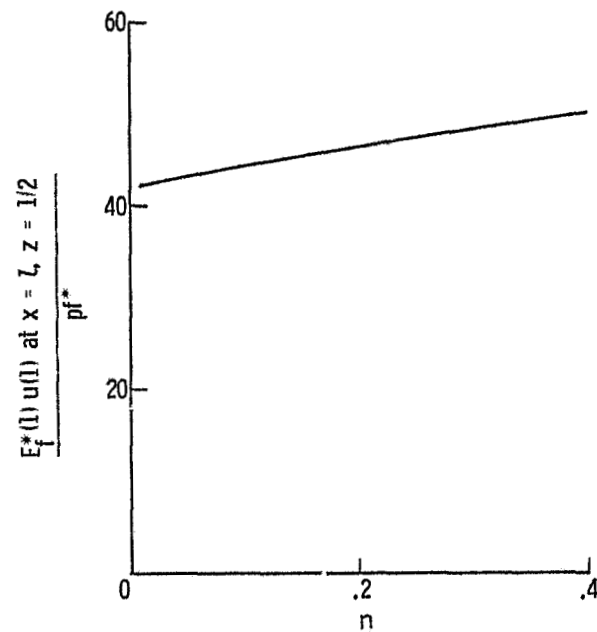
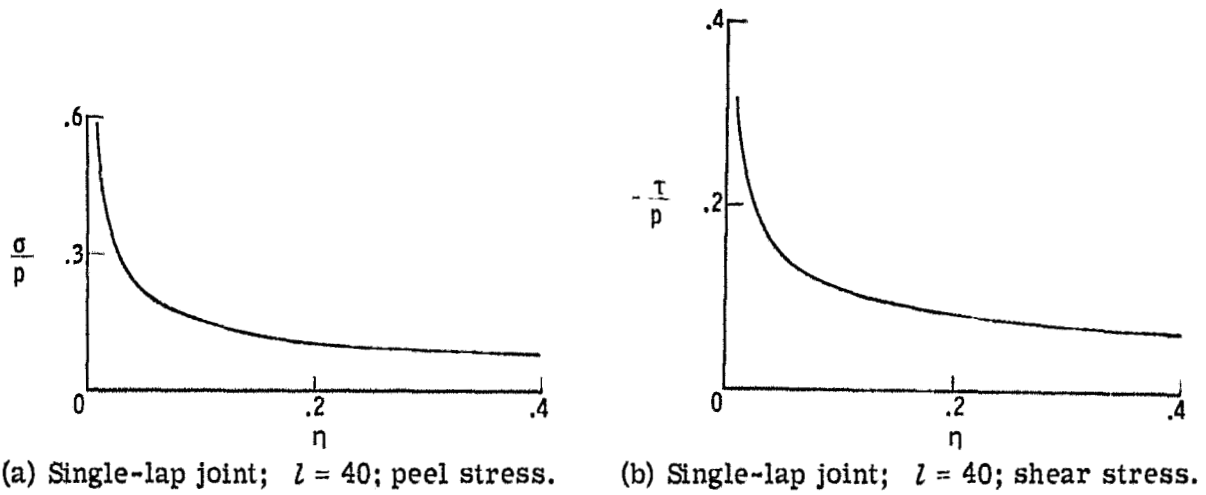
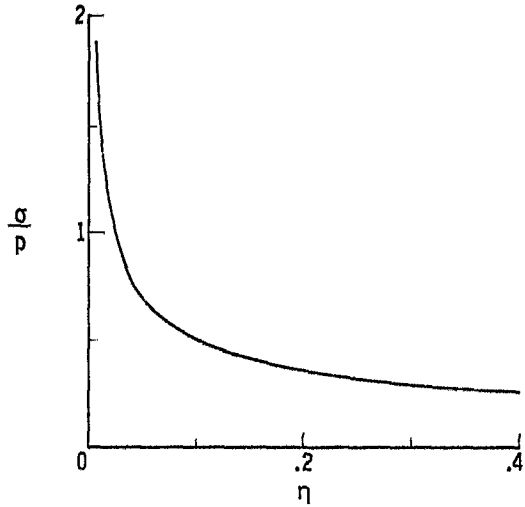
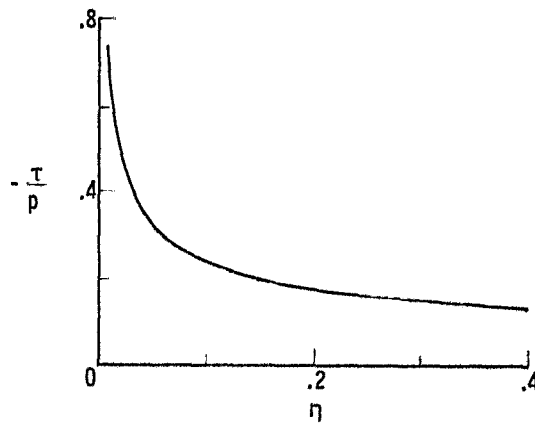


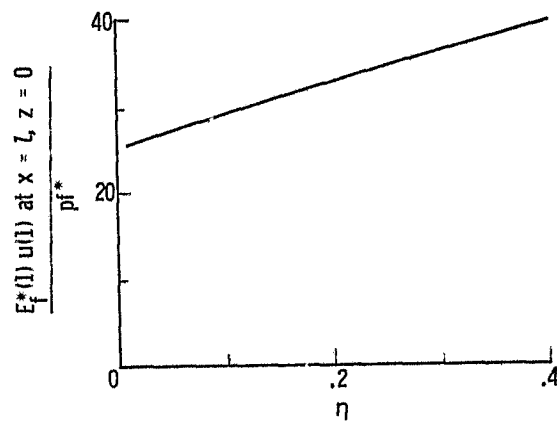
Figure 5.- Effect of adhesive thickness on maximum peel and shear stresses in bond and joint flexibility. Plates are of same material and same constant thickness.



(d) Flush joint;  $l = 20$ ; peel stress.

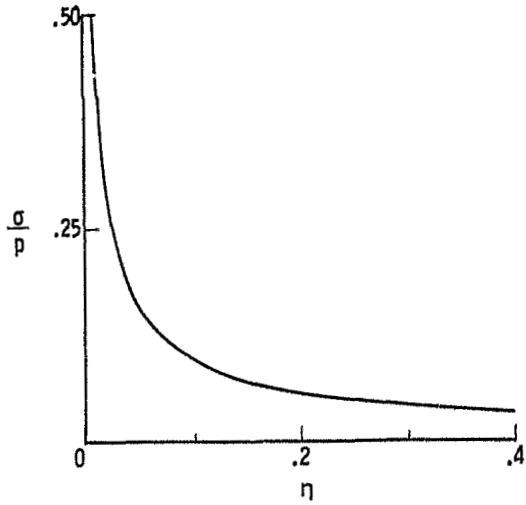


(e) Flush joint;  $l = 20$ ; shear stress.

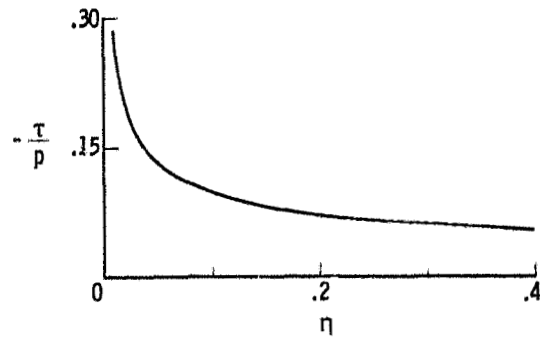


(f) Flush joint;  $l = 20$ ; joint flexibility.

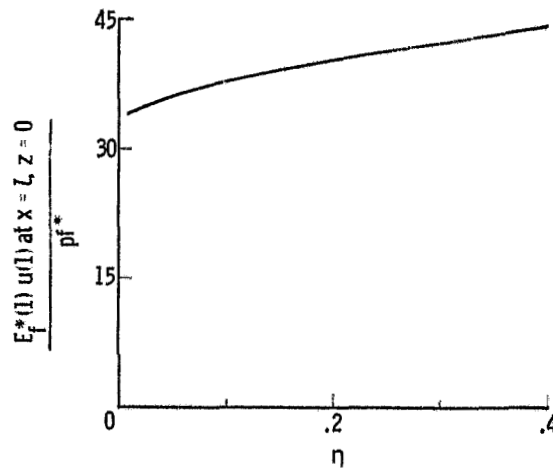
Figure 5.- Continued.



(g) Double-lap joint;  $l = 40$ ; peel stress.

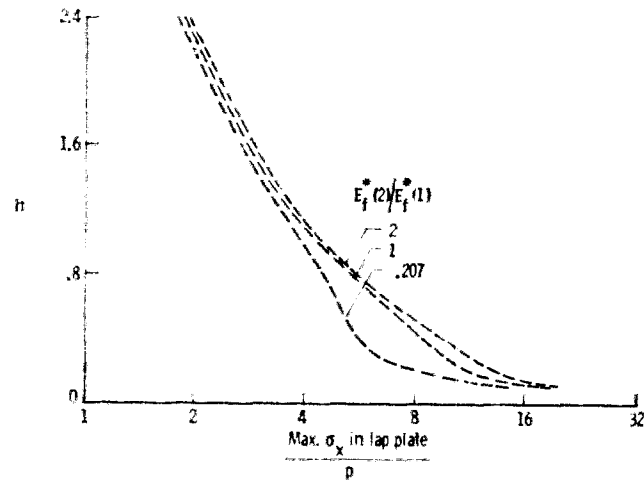


(h) Double-lap joint;  $l = 40$ ; shear stress.  
( $\tau$  at outer end is plotted because maximum peel stress occurs there, although  $\tau$  at inner end is slightly higher.)

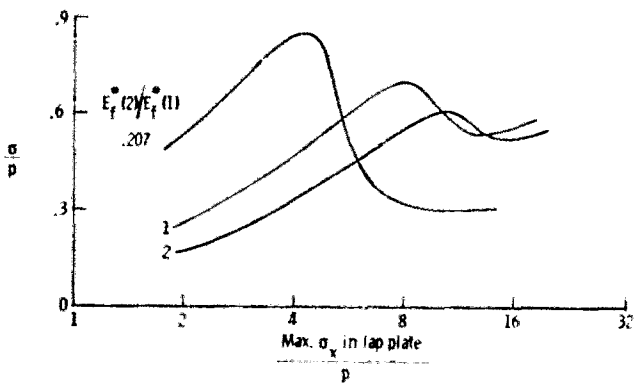


(i) Double-lap joint;  $l = 40$ ; joint flexibility.

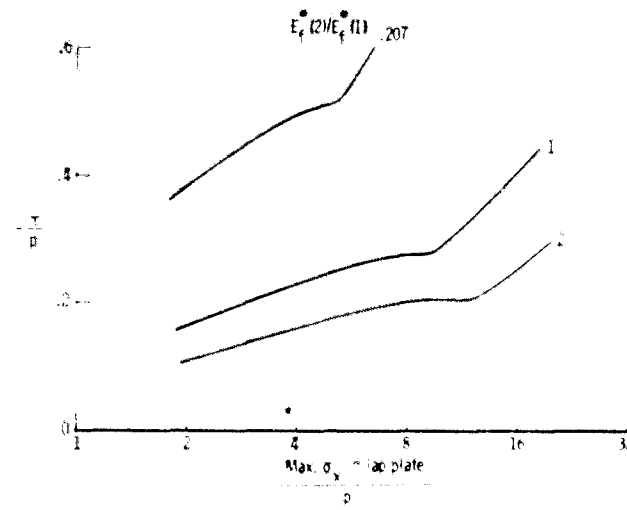
Figure 5.- Concluded.



(a) Flush joint;  $l = 20$ ;  $\eta = 0.1$ ; lap-plate thickness.

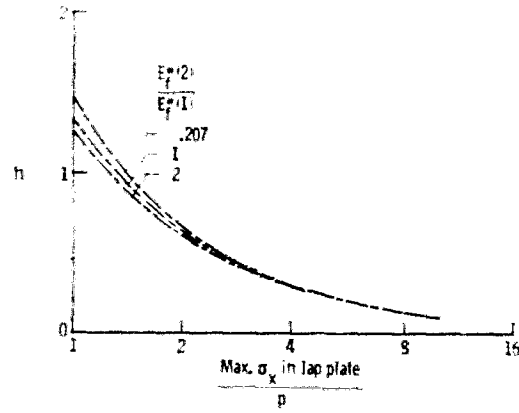


(b) Flush joint;  $l = 20$ ;  $\eta = 0.1$ ; peel stress.

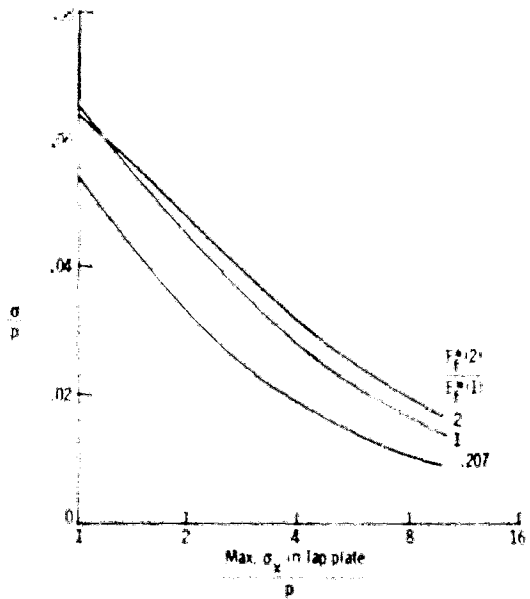


(c) Flush joint;  $l = 20$ ;  $\eta = 0.1$ ; shear stress.

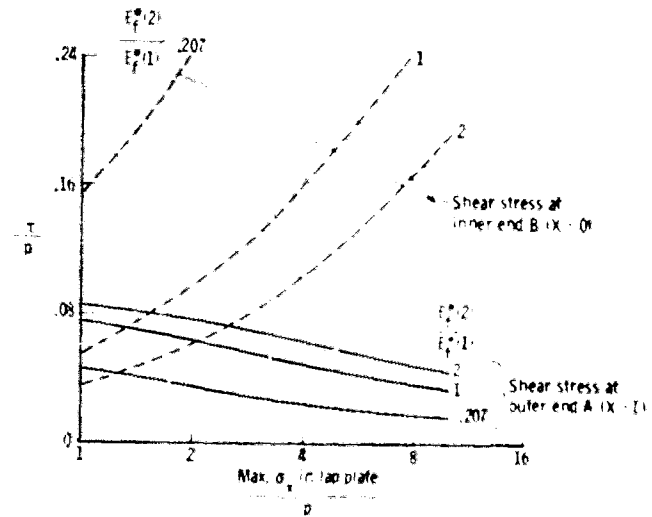
Figure 6.- Thickness of lap plate and maximum peel and shear stresses in bond as function of maximum direct stress in lap plate. Plates are of constant thickness.



(d) Double-lap joint;  $l = 40$ ;  $\eta = 0.2$ ; lap-plate thickness.

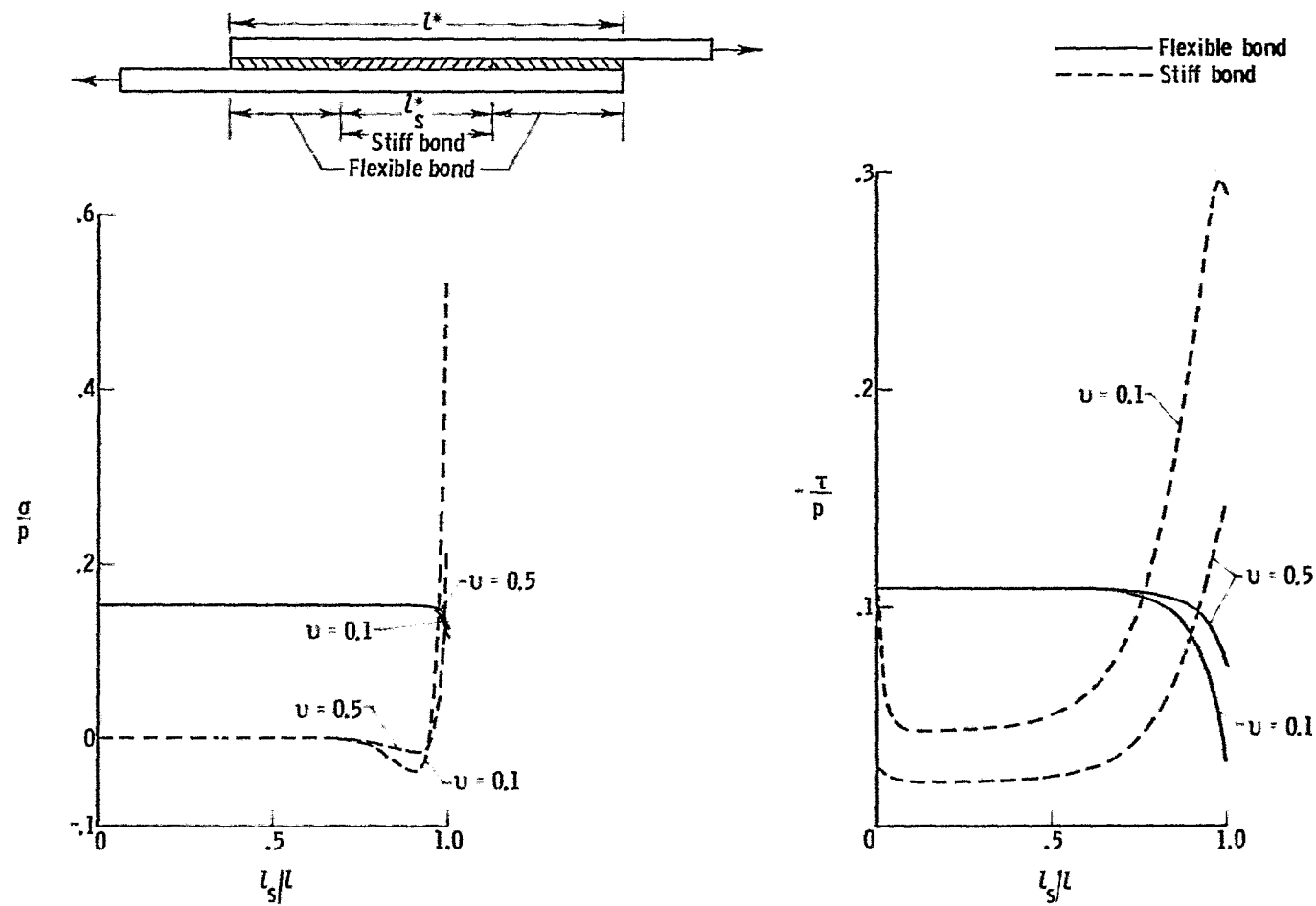


(e) Double-lap joint;  $l = 40$ ;  $\eta = 0.2$ ; peel stress.



(f) Double-lap joint;  $l = 40$ ;  $\eta = 0.2$ ; shear stress.

Figure 6.- Concluded.

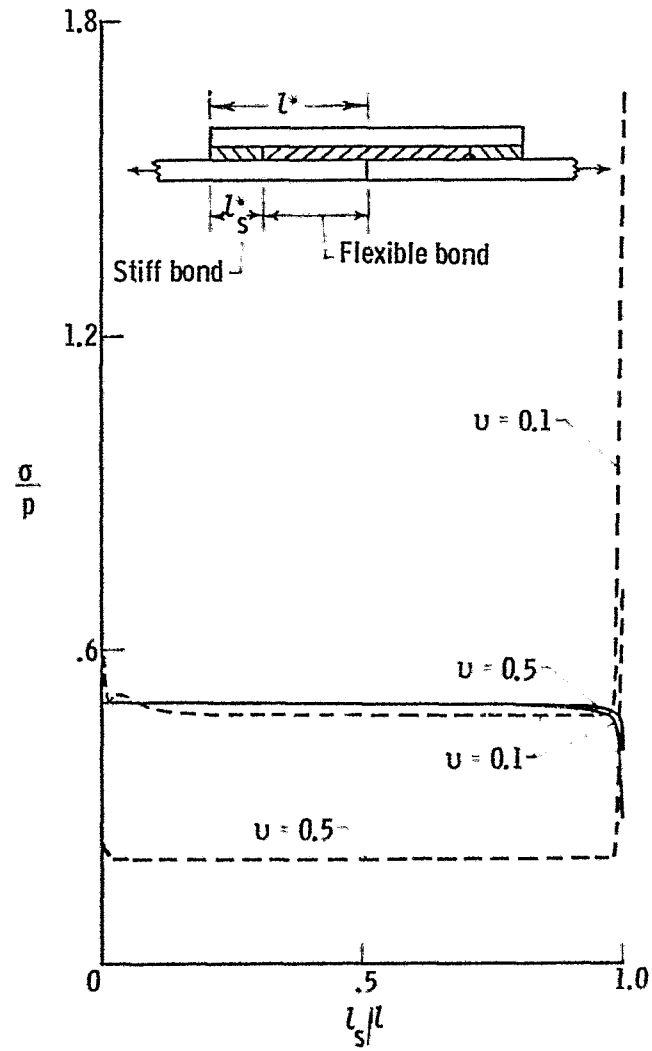


(a) Single-lap joint;  $l = 40$ ;  $\eta(\text{flexible bond}) = 0.1$ ; peel stress.

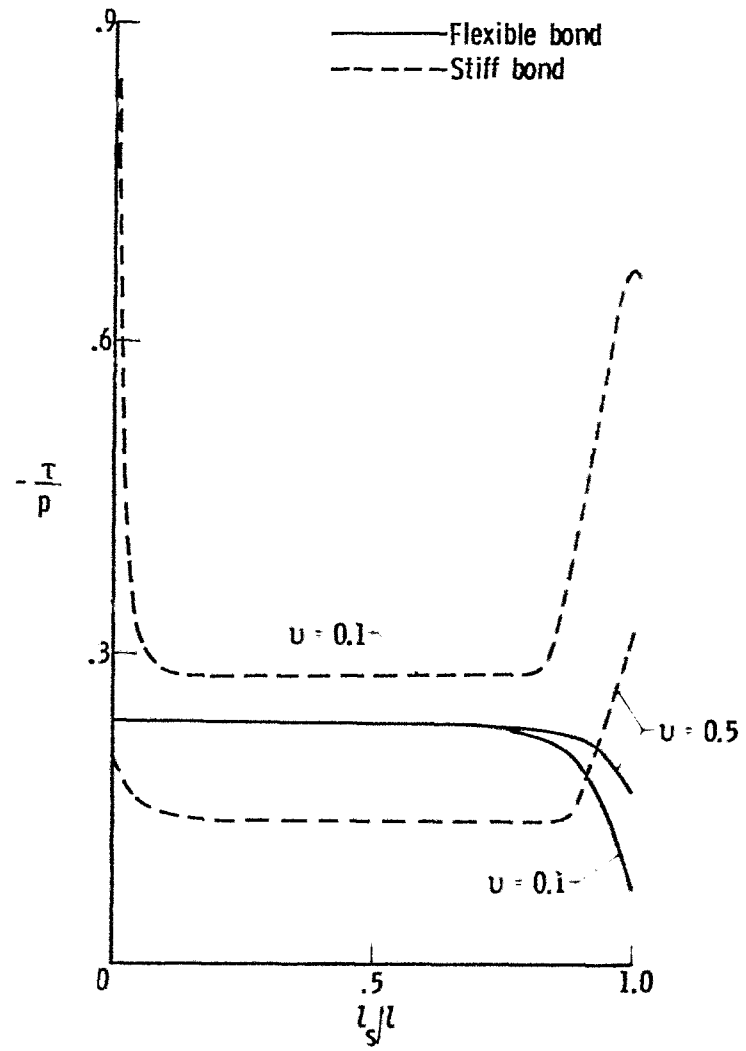
(b) Single-lap joint;  $l = 40$ ;  $\eta(\text{flexible bond}) = 0.1$ ; shear stress.

Figure 7.- Effect of using flexible and stiff bonds together on maximum peel and shear stresses in bond.

Plates are of same material and same constant thickness.  $\nu = \frac{k_x(\text{flexible bond})}{k_x(\text{stiff bond})} = \frac{k_z(\text{flexible bond})}{k_z(\text{stiff bond})}$ .

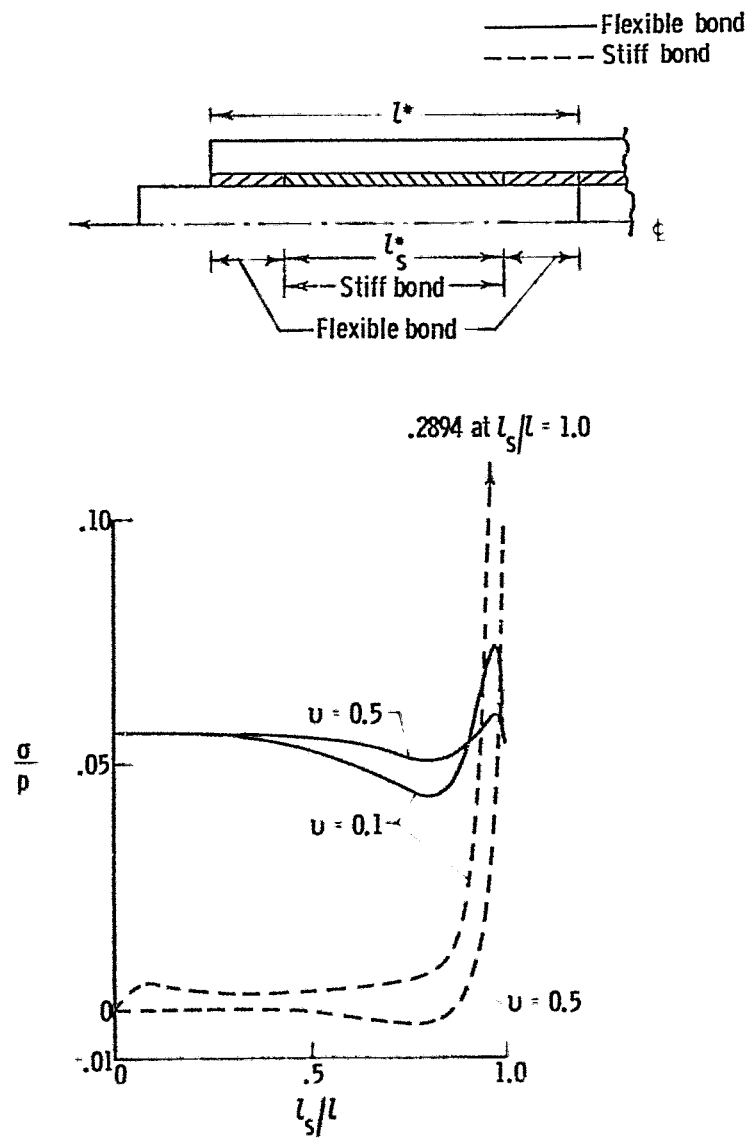


(c) Flush joint;  $l = 20$ ;  $\nu$ (flexible bond) = 0.1; peel stress.

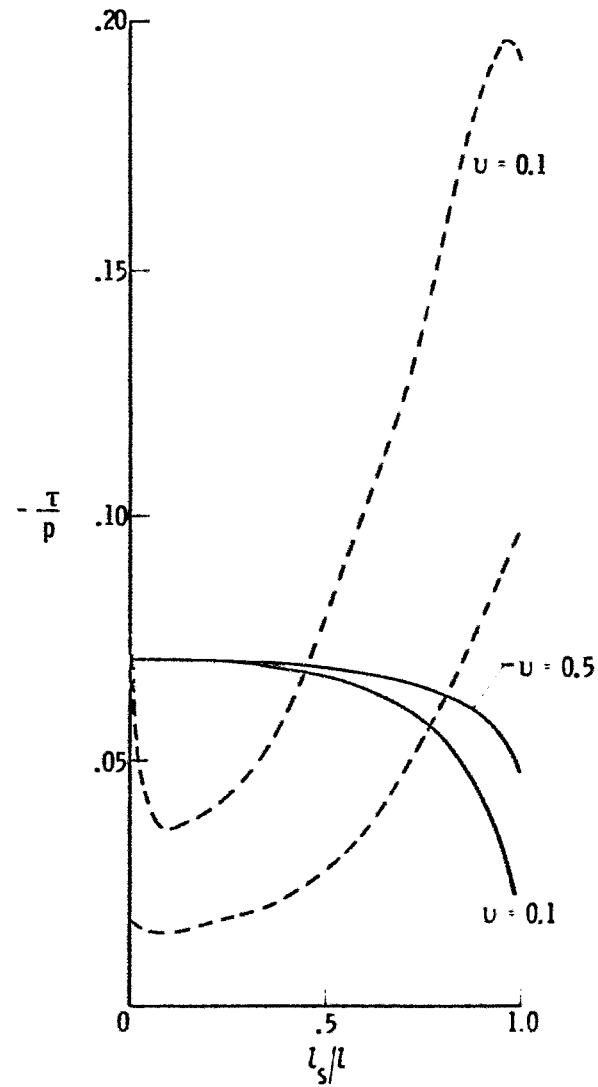


(d) Flush joint;  $l = 20$ ;  $\eta$ (flexible bond) = 0.1; shear stress.

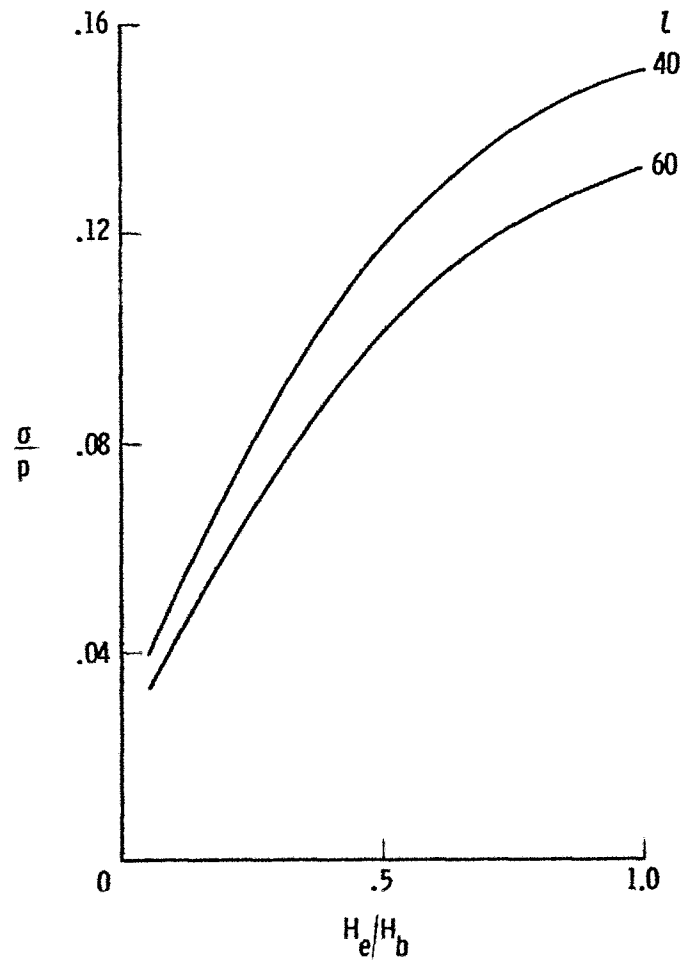
Figure 7.- Continued.



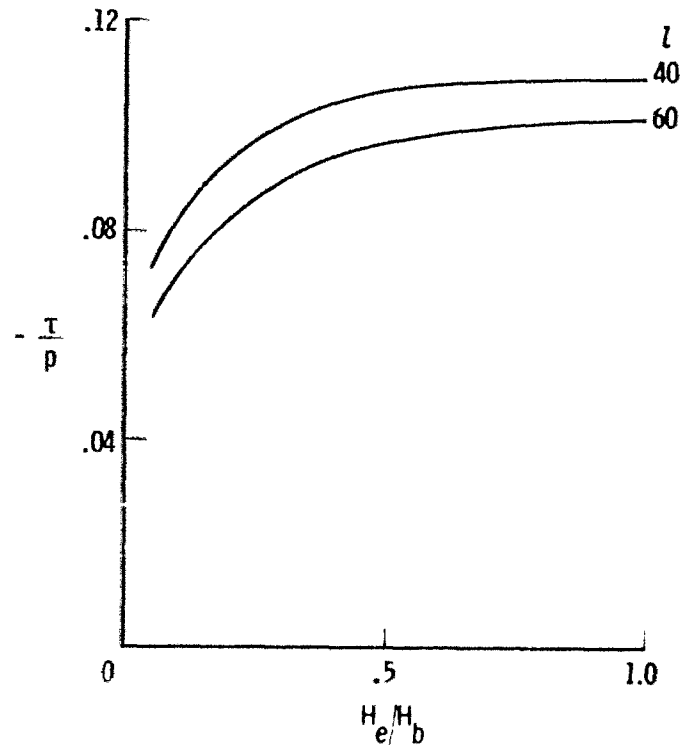
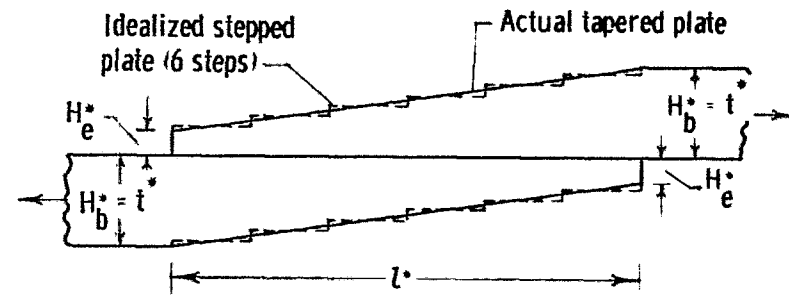
(e) Double-lap joint;  $l = 40$ ;  $\eta(\text{flexible bond}) = 0.2$ ;  
peel stress.



(f) Double-lap joint;  $l = 40$ ;  $\eta(\text{flexible bond}) = 0.2$ ;  
shear stress.

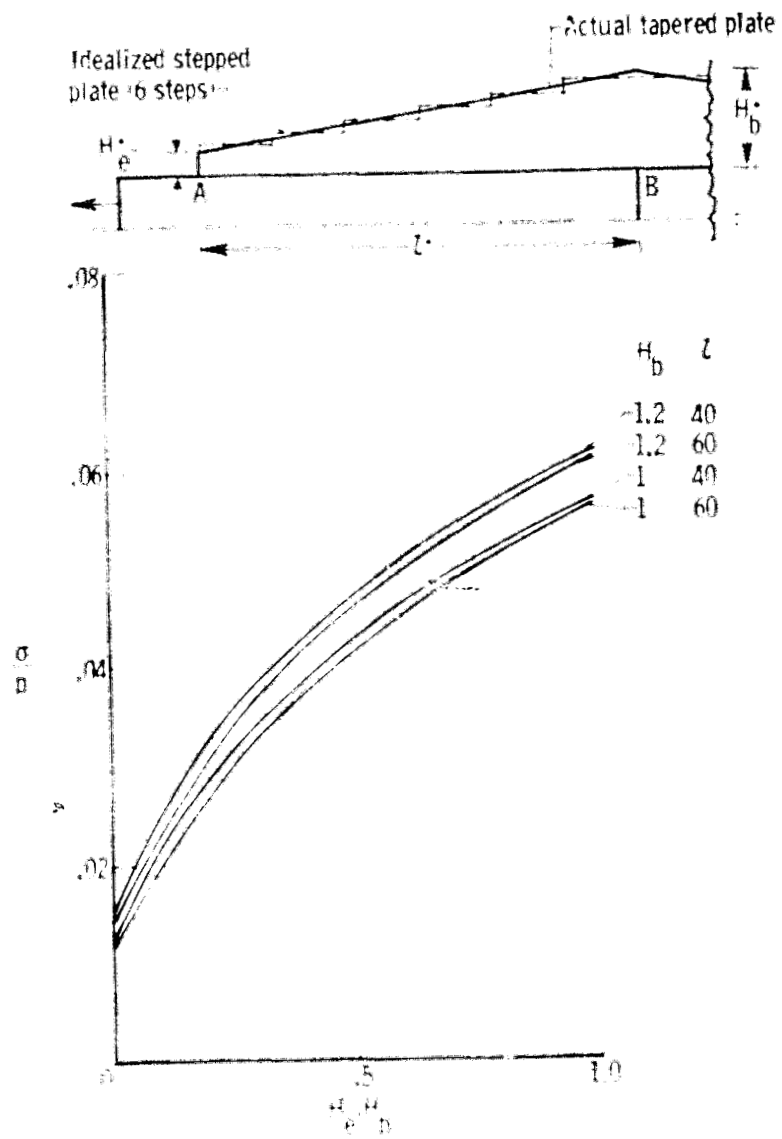


(a) Single-lap joint;  $\eta = 0.1$ ;  $H_b = 1$ ; peel stress.

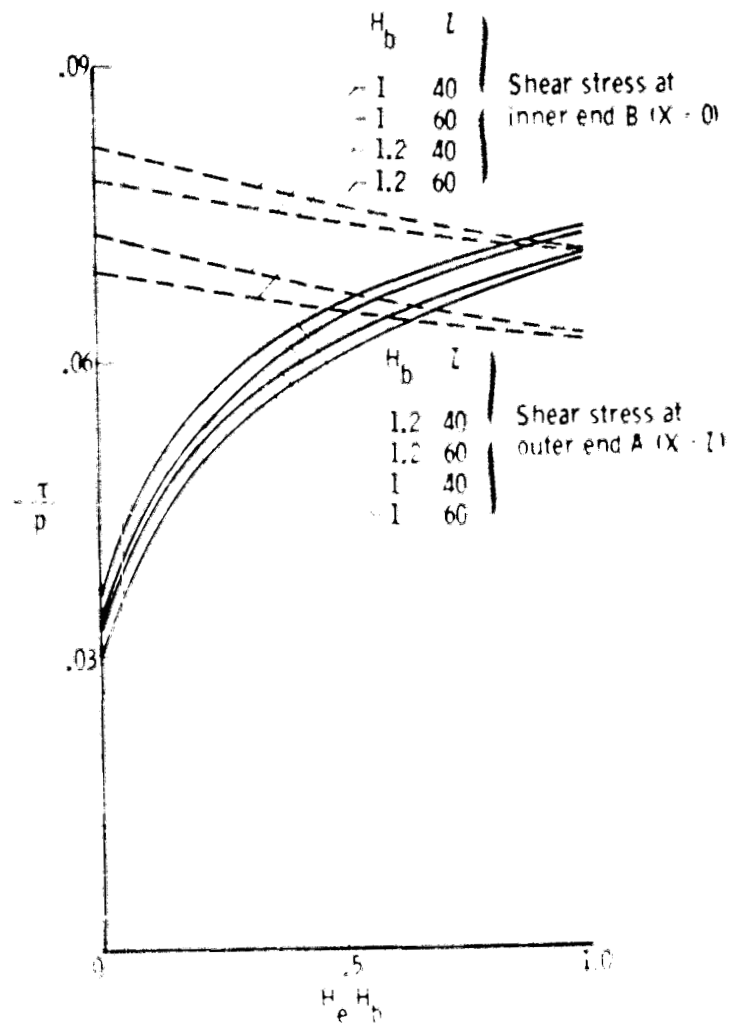


(b) Single-lap joint;  $\eta = 0.1$ ;  $H_b = 1$ ; shear stress.

Figure 8.- Effect of plate taper on maximum peel and shear stresses in bond. Plates are of same material.



(c) Double-lap joint:  $\gamma = 0.2$ : peel stress.



(d) Double-lap joint:  $\gamma = 0.2$ : shear stress.

Figure 8.- Concluded.

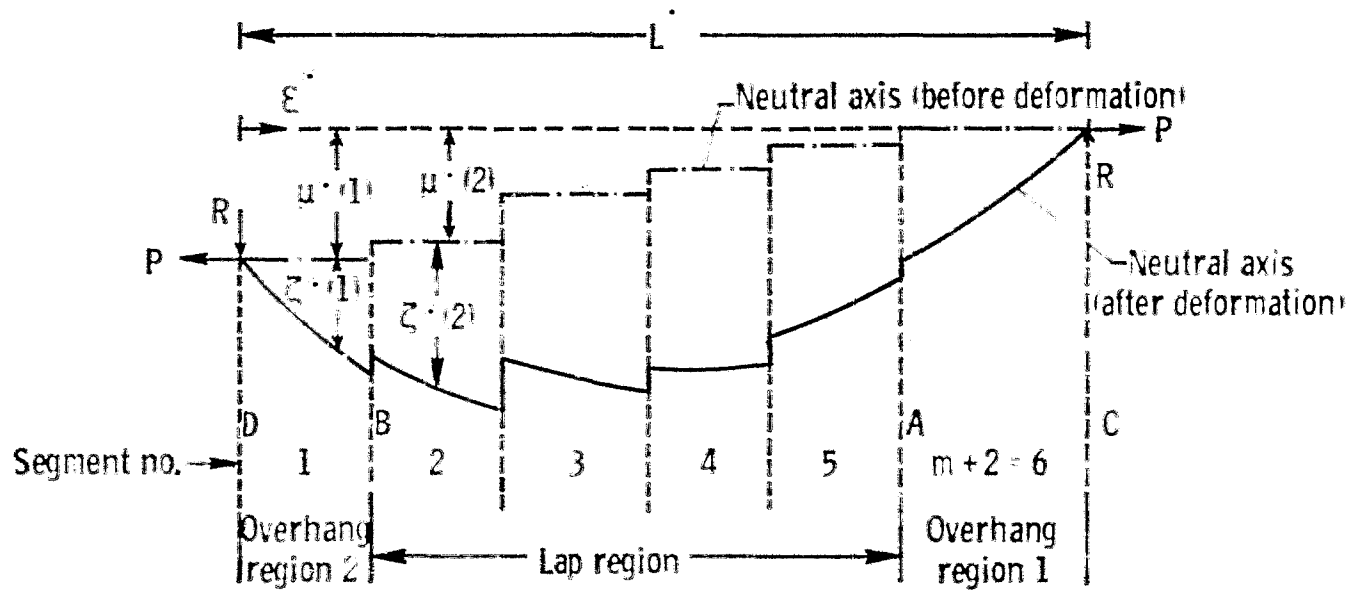


Figure 9.- Coordinate system for analysis of effects of large deflections on single-lap or flush joints. (For illustration, a joint with four steps is considered.)